

RESEARCH ARTICLE

10.1029/2018JB016199

Key Points:

- Seventeen years of degassing, thermal, deformation, and Global Volcanism Program ground-based data are analyzed for the 47 most active volcanoes in Latin America
- This study demonstrates the advantages of using a multiparameter approach for monitoring volcanoes while demonstrating the need for greater coordination
- The data are used to test the open and closed volcanic classification scheme, demonstrating the need for additional classifications

Supporting Information:

- Supporting Information S1
- Table S1
- Table S2
- Table S3
- Table S4
- Table S5

Correspondence to:

K. Reath,  
kar287@cornell.edu

Citation:

Reath, K., Pritchard, M., Poland, M., Delgado, F., Carn, S., Coppola, D., et al. (2019). Thermal, deformation, and degassing remote sensing time series (CE 2000–2017) at the 47 most active volcanoes in Latin America: Implications for volcanic systems. *Journal of Geophysical Research: Solid Earth*, 124, 195–218. <https://doi.org/10.1029/2018JB016199>














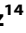




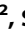

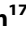

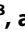

Received 8 JUN 2018

Accepted 1 DEC 2018

Accepted article online 5 DEC 2018

Published online 12 JAN 2019

# Thermal, Deformation, and Degassing Remote Sensing Time Series (CE 2000–2017) at the 47 most Active Volcanoes in Latin America: Implications for Volcanic Systems

K. Reath<sup>1</sup> , M. Pritchard<sup>1</sup> , M. Poland<sup>2</sup> , F. Delgado<sup>1,3</sup> , S. Carn<sup>4</sup> , D. Coppola<sup>5</sup> , B. Andrews<sup>6</sup> , S. K. Ebmeier<sup>7</sup> , E. Rumpf<sup>8</sup> , S. Henderson<sup>9</sup> , S. Baker<sup>10</sup> , P. Lundgren<sup>11</sup> , R. Wright<sup>12</sup> , J. Biggs<sup>13</sup> , T. Lopez<sup>14</sup> , C. Wauthier<sup>15</sup> , S. Moruzzi<sup>1</sup> , A. Alcott<sup>1</sup> , R. Wessels<sup>16</sup> , J. Griswold<sup>2</sup> , S. Ogburn<sup>2</sup> , S. Loughlin<sup>17</sup> , F. Meyer<sup>14</sup> , G. Vaughan<sup>8</sup> , and M. Bagnardi<sup>7,11</sup> 

<sup>1</sup>Earth and Atmospheric Sciences, Cornell University, Ithaca, NY, USA, <sup>2</sup>U.S. Geological Survey – Cascades Volcano Observatory, Vancouver, WA, USA, <sup>3</sup>Équipe de Tectonique et Mécanique de la Lithosphère, Institut de Physique du Globe de Paris, Paris, France, <sup>4</sup>Geological and Mining Engineering and Sciences, Michigan Technological University, Houghton, MI, USA, <sup>5</sup>Department of Earth Sciences, Università Delgi Studi di Torino, Torino, Italy, <sup>6</sup>Mineral Sciences, Smithsonian Institution, Washington, DC, USA, <sup>7</sup>School of Earth and Environment, University of Leeds, Leeds, UK, <sup>8</sup>U.S. Geological Survey – Astrogeology Science Center, Flagstaff, AZ, USA, <sup>9</sup>Earth and Space Sciences, University of Washington, Seattle, WA, USA, <sup>10</sup>University NAVSTAR Consortium (UNAVCO), Boulder, CO, USA, <sup>11</sup>Jet Propulsion Laboratory (JPL), California Institute of Technology, Pasadena, CA, USA, <sup>12</sup>Hawai'i Institute of Geophysics and Planetology, University of Hawaii at Manoa, Honolulu, HI, USA, <sup>13</sup>School of Earth Sciences, University of Bristol, Clifton, UK, <sup>14</sup>Geophysical Institute, University of Alaska Fairbanks, Fairbanks, AK, USA, <sup>15</sup>Department of Geosciences, Pennsylvania State University, University Park, PA, USA, <sup>16</sup>U.S. Geological Survey Headquarters, Reston, VA, USA, <sup>17</sup>British Geological Survey, The Lyell Centre, Edinburgh, Scotland

**Abstract** Volcanoes are hazardous to local and global populations, but only a fraction are continuously monitored by ground-based sensors. For example, in Latin America, more than 60% of Holocene volcanoes are unmonitored, meaning long-term multiparameter data sets of volcanic activity are rare and sparse. We use satellite observations of degassing, thermal anomalies, and surface deformation spanning 17 years at 47 of the most active volcanoes in Latin America and compare these data sets to ground-based observations archived by the Global Volcanism Program. This first comparison of multisatellite time series on a regional scale provides information regarding volcanic behavior during, noneruptive, pre-eruptive, syneruptive, and posteruptive periods. For example, at Copahue volcano, deviations from background activity in all three types of satellite measurements were manifested months to years in advance of renewed eruptive activity in 2012. By quantifying the amount of degassing, thermal output, and deformation measured at each of these volcanoes, we test the classification of these volcanoes as open or closed volcanic systems. We find that ~28% of the volcanoes do not fall into either classification, and the rest show elements of both, demonstrating a dynamic range of behavior that can change over time. Finally, we recommend how volcano monitoring could be improved through better coordination of available satellite-based capabilities and new instruments.

## 1. Introduction

Volcanic eruptions pose a risk to the life and livelihood of local communities by damaging infrastructure and displacing populations and can have global impacts by disrupting climate, businesses, and air travel (e.g., Brown, Sparks, et al., 2015; Loughlin et al., 2015; Ridley et al., 2014). Eruptive hazards include, but are not limited to, ash clouds, volcanic bombs, pyroclastic flows, lava flows, lahars, debris avalanches, and magma intrusion-induced earthquakes (e.g., Blong, 2013; Wauthier et al., 2013, 2015). There are ~1,400 subaerial Holocene volcanoes around the world, and Brown, Auken, et al. (2015) found that 800 million people are estimated to live within 100 km, and about 30 million people within 10 km, of these volcanoes. These distances are within the striking distance of the hazards associated with large volcanic eruptions, and even small to moderate eruptions could affect the people who live within 10 km (Brown, Auken, et al., 2015).

Many, but not all, volcanic eruptions are preceded by some form of unrest, including increased seismic activity, ground deformation, gas emissions, and thermal anomalies (e.g., Barberi et al., 1984; Newhall, 2000; Potter et al., 2015; Reath et al., 2016). Long-term monitoring is the best means of recognizing these signs of unrest and determining whether they are anomalous, particularly if they are indicative of an

impending eruption (e.g., Phillipson et al., 2013), or changing hazards during an eruption (e.g., Segall, 2013; Sparks, 2003). However, to determine whether activity is anomalous, a baseline for background behavior must be established. Additionally, volcanic unrest does not always manifest in the same manner or consistently lead to eruption and therefore should be monitored using multiple techniques (National Academies of Sciences, 2017).

For past eruptive events, multidiscipline ground-based measurements of seismic activity, ground deformation, gas/aerosol emissions, and thermal anomalies have provided crucial information for tracking volcanic unrest (e.g., Kauahikaua & Poland, 2012; Mothes et al., 2015; Wadge & Aspinall, 2014; Wadge et al., 2014). In fact, increased instrumentation has been shown to improve both eruption forecasting (Cameron et al., 2018) and alert-level assignment during volcanic crises (e.g., Winson et al., 2014). Unfortunately, ground-based monitoring instruments are available at less than half of the volcanoes considered to be potentially active (e.g., Brown, Sparks, et al., 2015). Among these ground-monitored volcanoes, many lack the array of instrumentation needed to provide multidisciplinary information, due to a lack of resources, lack of access in remote locations, and the danger inherent to being close to an active volcano. Improved monitoring is possible by utilizing available satellite resources, which can provide information on ground deformation, gas and aerosol emissions, and thermal anomalies at all ~1,400 subaerial volcanoes (e.g., Bally, 2012; Biggs et al., 2014; Carn et al., 2017; Wright, 2016).

We focus on *three types* of remote sensing observations that provide insights into the processes occurring within a volcanic system. *SO<sub>2</sub> emissions* reflect the mass and relative depth of magma degassing, the permeability of the conduit, and can be used to identify magma recharge (e.g., Caltabiano et al., 1994; Galle et al., 2010; Symonds et al., 1994). *Thermal data* can be used to identify volcanogenic heating, variations in which have been related to pre-eruptive activity (e.g., Dehn et al., 2002; Pieri & Abrams, 2005; Reath et al., 2016). During eruptions, thermal data have been used to estimate lava discharge rates (Coppola et al., 2009; Harris et al., 2000, 1998) and, in some cases, to forecast the end of an effusive eruption (e.g., Bonny & Wright, 2017; Coppola et al., 2017; Ripepe et al., 2017). *Interferometric SAR (InSAR) data* are processed from Synthetic Aperture Radar (SAR) data, which measures changes in surface characteristics over time with all-weather, day-night capability. InSAR can provide information on pre-eruptive, syneruptive, and post-eruptive deformation (e.g., Biggs et al., 2014; Biggs & Pritchard, 2017). SAR amplitude imagery is also valuable for assessing changes in volcanic morphology over time—for example, SAR data were used to measure the growth rate of the lava dome at Merapi Indonesia, in 2010. The results aided assessments that prompted evacuations credited with saving thousands of lives (Pallister et al., 2012).

Despite this potential, there are challenges to using multisatellite remote sensing observations to study volcanoes on a global basis. Processing remote sensing data requires specialized knowledge and software, and each data set has unique characteristics (Table 1). The detection threshold of unrest is limited by the magnitude of unrest as well as the spatial resolution of the measurement (i.e., pixel size), temporal resolution of the instrument (i.e., repeat time of observations), and the sensitivity of the sensor (i.e., ability to detect minute changes above ambient background data values). In addition, remote sensing techniques are often used in isolation by specialized groups or individuals (e.g., Carn et al., 2016; Meyer et al., 2016; Wright, 2016), despite the fact that manifestations of volcanic unrest are interrelated. This study seeks to demonstrate the potential of systematically integrating multiple remote sensing data sets to better recognize processes associated with volcanic unrest and eruption.

Here we present the first multidecadal (17 years) and multiparameter time series synthesis of remote sensing observations of volcanic degassing, thermal activity, and deformation on a regional scale, with the goal of demonstrating the utility of using multiple satellite data sets to understand the manifestations of volcanic unrest and eruption. These data have been compiled from published literature, and, where needed, new data collections and analysis were conducted to fill gaps in spatial, temporal, and sensor coverage. We target 47 volcanoes in Latin America (Figure 1) and, where possible, compare our satellite observations to ground observations. By incorporating multiple data types, temporal variations in activity identified by one type of technique can be reinforced by complementary cotemporal observations in other techniques. A specific goal is to assess the capabilities of these data to establish pre-eruptive trends and to determine how consistently they can act as indicators of eruption (e.g., Biggs & Pritchard, 2017; Carn et al., 2016; Jay et al., 2013; Pieri & Abrams, 2005; Reath et al., 2016). Further, we aim to investigate both individual and regional volcanic

**Table 1**

*Satellite Sensors That Contributed to Degassing (Rows 1–4), Thermal (Rows 5 and 6) and Deformation (Remaining Rows) Data Sets Used in the Time Series (Figures 2, 4, 5, 6, and Figures S1–S47 in the Supporting Information)*

Sensor	Acronym	Launch date	Expiration date	Space agency
Infrared Atmospheric Sounding Instrument	IASI	October 2006	Current	Centre national d'études spatiales (CNES)
Total Ozone Mapping Spectrometer	TOMS	October 1978	May 1992	National Aeronautics and Space Administration (NASA)
Total Ozone Mapping Spectrometer-Earth Probe	TOMS_EP (TOMS)	July 1996	December 2006	NASA
Ozone Monitoring Instrument	OMI	January 2004	Current	Netherland's Agency for Aerospace Programs (NIVR)/ Finnish Meteorological Institute (FMI)
Advanced Spaceborne Thermal Emission and Reflection Radiometer	ASTER	December 1999	Current	NASA/ Japan's Ministry of Economy, Trade, and Industry (METI)/ Japan Space Systems
Moderate Resolution Imaging Spectroradiometer	MODIS	December 1999	Current	NASA
European Remote-Sensing Satellite	ERS-1	July 1991	March 2000	European Space Agency (ESA)
	ERS-2	April 1995	September 2011	
RADARSAT	RSAT-1	November 1995	March 2013	Canadian Space Agency (CSA)
	RSAT-2	December 2007	Current	
Advanced Land Observation Satellite	ALOS-1	January 2006	May 2011	Japan Aerospace Exploration Agency (JAXA)
	ALOS-2	May 2014	Current	
Environmental Satellite	ENVISAT	March 2002	April 2012	ESA
Constellation of Small Satellites for the Mediterranean basin Observation (COSMO)-SkyMed	CSK-1	June 2007	Current	Italian Space Agency (ASI)
	CSK-2	December 2007	Current	
	CSK-3	October 2008	Current	
	CSK-4	November 2010	Current	
Sentinel	Sentinel-1A	April 2014	Current	ESA
	Sentinel-1B	April 2016	Current	
TerraSAR-X	TSX	January 2008	Current	German Aerospace Center (DLR)
TanDEM-X	TDX	June 2010	Current	DLR

behaviors and to use these data sets to classify volcanoes using the established “open” or “closed” system definitions (e.g., Biggs et al., 2014; Chaussard et al., 2013; Chaussard & Amelung, 2014; C.G. Newhall, 2007; Oppenheimer et al., 1993) and identify if these classifications systematically change within the region.

### 1.1. Study Area: Latin America

As a step toward developing an international remote sensing geohazards monitoring effort, the Committee on Earth Observation Satellites (CEOS), an umbrella organization of major international space agencies dedicated to international coordination of space-based Earth observations, initiated a series of pilot projects for geohazards (specifically volcanoes, earthquakes, floods, and landslides). The volcano pilot project focused on a regional study of volcanic unrest and eruption in Latin America during 2014–2017 to demonstrate a proof of concept for a global volcano observatory in space, resulting in an increase in availability of SAR data in this region (Pritchard et al., 2018). The project chose Latin America as a test area due to its abundant volcanic activity and wide diversity of environmental conditions. Volcanoes within this region exhibit a variety of eruption styles—including Strombolian to Plinian explosions, lava lakes, and episodic to continuous effusion of basaltic to rhyolitic magma from both open and closed systems (e.g., Chaussard et al., 2013; Newhall, 2007). Additionally, eruptions in this region strongly impact local populations and regional air traffic, yet they are undermonitored by ground-based methods (Pritchard et al., 2018). This study focuses on the most active volcanoes in Latin America (Figure 1). However, we acknowledge that our sample size is of limited area; thus, some volcano types or environments will be underrepresented. Additionally, a majority of the volcanoes in this study are in a continental margin arc. Outcomes related to open and closed systems as well as other topics may well be different in other areas (e.g., intraoceanic arc and continental rift).



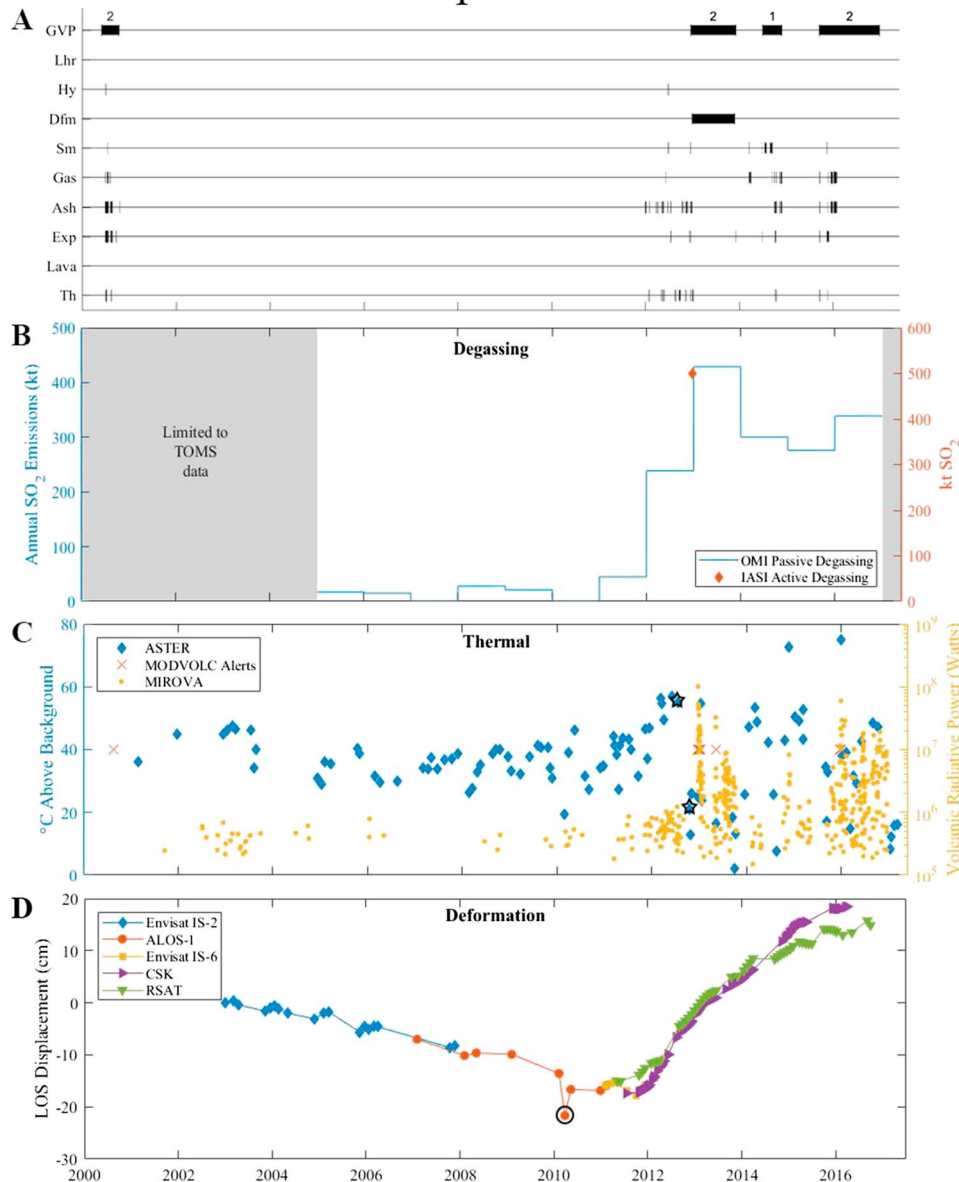
**Figure 1.** Map of the locations and names of all 47 Latin American volcanoes included in this study.

The 47 volcanoes of interest exhibit previously detected unrest that, in many cases, culminated in an eruption. These are a subset of the more than 60 volcanoes in Latin America considered restless, including those with eruptions since 2000 (49), those that have experienced seismic swarms without eruption (9), or other satellite detected unrest (54) since 1990 (Pritchard et al., 2018). We have excluded most volcanoes where only one data type exhibited unrest or detections are not clearly related to subsurface magmatic and/or hydrothermal processes (see Table S1). For example, we do not include subsidence at Parícutin volcano and Lonquimay volcanoes that has been related to cooling of lava flows (Chaussard, 2016; Delgado et al., 2017; Fournier et al., 2010). We also do not include deformation at volcanoes related to gravity-controlled flank creep (Ebmeier et al., 2010), flow subsidence (Schaefer et al., 2016), or volcanoes that only deformed during the Mw 8.8 Maule earthquake (Pritchard et al., 2013).

## 2. Methods

Four data types are compiled (where available) for each volcano in this study (example of Copahue volcano in Figure 2): (A) ground-based volcano monitoring data compiled from the Bulletin of the Global Volcanism Network (BGVN) provided by the Smithsonian Institute Global Volcanism Program (GVP) (Venzke, 2013), (B)

# Copahue



**Figure 2.** All available degassing, thermal, deformation, and GVP compiled ground-based data for Copahue volcano (on the Argentina-Chile border). Similar plots were compiled for all 47 Latin American volcanoes of interest. (a) Ground-based monitoring derived from BGVN data; abbreviations are as follows: GVP = eruption timing as indicated by the GVP, numbers in this category correspond to volcanic explosivity index (VEI; Newhall & Self, 1982) values of eruption determined by the GVP, Lhr = lahars, Hy = hydrothermal event, Dfm = deformation, Sm = seismicity, Gas = gas emission, Ash = ash emission, Exp = explosive eruption, Lava = effusive eruption, Th = thermal anomaly. Black vertical bars indicate times where activity types have been noted. (b) Satellite-based SO<sub>2</sub> emission masses (kt) from the OMI sensor (Carn et al., 2016, 2017). Gray-shaded areas designate times when data are limited. Before 2005, there are no OMI data, and only TOMS SO<sub>2</sub> emission information, with lowered sensitivity and spatial resolution is available; no data were analyzed for 2017. Passive degassing is represented as a bar averaged over a year, whereas active degassing from discrete measurements are represented by a single point (these are typically associated with explosive eruptions). (c) Satellite-based thermal data. ASTER data are measured in °C above background (left axis), whereas the Middle InfraRed Observation of Volcanic Activity (MIROVA) volcanic radiative power data (Coppola et al., 2016) are measured in Watts (right axis). The temperatures (section 2.3) from the two ASTER images shown in Figure S48. (i.e., 24 July and 10 October 2012) have been surrounded by black stars. The MODVOLC alert data provide information on the timing of the alerts (when a band ratio exceeds a threshold; Wright, Flynn, et al., 2004; Wright, Parsons, et al., 2004) and are always plotted in the center of the y-axis. (d) Satellite-based deformation data. Data acquired from different sensors are marked separately. Envisat data are interpreted from Velez et al. (2016), ALOS, CSK, and RSAT-2 data (the latter two from Lundgren et al., 2017) are from the point  $-37.838$  (latitude),  $-71.171$  (longitude). We found previously unreported subsidence at Copahue associated with the 2010 Maule earthquake occurring before 26 March 2010 and surrounded by a black circle, which is similar to the subsidence documented at five other Latin American volcanoes (Pritchard et al., 2013). The CSK and RSAT time series have some slight differences from 17 July to 6 June 2012 and from 29 March 2014 to 29 March 2016 (section 3.1). This is likely due to the 12° difference in look angle between these two instruments, which would have an effect on line-of-sight (LOS) measurements.

multisatellite observations of SO<sub>2</sub> degassing, (C) thermal output measured from space, and (D) satellite observations of ground deformation. All of the raw data used to make the plots have been provided to WOVodat (Newhall et al., 2017) and now populate their volcanic unrest database. We selected a start date of 1 January 2000 and end date of 1 June 2017, although not all sensors provided usable data at all volcanoes during this time span. Setting the same defined time period provides a uniform format for data plots, facilitating comparison between volcanoes. Details about data sources and their limitations are provided in the following sections.

### 2.1. Ground-Based Observations

To incorporate ground-based observations into our data sets, we constructed timelines of volcanic activity from BGVN reports and the Volcanoes of the World (VOTW) databases. Specifically, we pulled individual events and periods of activity from the BGVN narrative descriptions and assigned start and end dates. Events were classified into nine different types: lahars, hydrothermal (including changes in crater lakes or hydrothermal systems), deformation, elevated seismicity (including tremor or earthquake swarms), gas emission, ash emission, explosive eruption (including magmatic, phreatomagmatic, or phreatic), lava effusion, and thermal/incandescence (Figure 2a). The majority of the observations describing these events in BGVN are ground based, but some satellite observations are also included (e.g., some BGVN reports include MODIS alerts and InSAR data; however, reporting methods are not consistent). Wherever the type of activity is reported, it is included independent of scale (e.g., a small ash puff is given the same value as a large ash cloud). We note that as the BGVN relies heavily upon reporting by observatories, these reports contain observation biases and omissions based on the degree of instrumentation available and the threshold for reporting at the specific observatory. There is undoubtedly volcanic activity that is absent from the timelines (e.g., seismicity at volcanoes with no seismic network would not be reported). Further, the BGVN does not always receive and record all the data collected and used by volcano observatories.

In Figure 2a, the “GVP” row is used to track eruptive periods. The start dates of eruptions correspond with the first appearance of new ejecta or lava as reported in the BGVN. Any eruption of tephra or lava occurring within a 3-month period following the start date is considered to be part of the same eruptive event. The numbers used in this row correspond with the eruption’s volcanic explosivity index (VEI) value, which is based upon the largest volume of ejecta produced during any one eruption during the period (Newhall & Self, 1982). For simplicity, rather than citing each BGVN report, we cite the VOTW database (Venzke, 2013), which contains those individual reports, and the profile webpage for each volcano from which the reports can be accessed.

### 2.2. Degassing

The satellite derived volcanic SO<sub>2</sub> measurements presented here are from Carn et al. (2016, 2017) and Theys et al. (2013) and were acquired using two methods depending on the style of emissions—active (e.g., emissions detected during an eruption) and passive (e.g., emissions detected during noneruptive periods). For active SO<sub>2</sub> emissions, which were released and measured during explosive and effusive eruptions, the maximum SO<sub>2</sub> mass measured from a single satellite acquisition is reported in kilotons (kt), following the methods of Carn et al. (2016). We assume this to represent the total SO<sub>2</sub> mass released during that eruption and is limited to emissions contained within the upper troposphere to the lower stratosphere. These measurements were acquired using a variety of ultraviolet and infrared sensors (Table 1), with SO<sub>2</sub> masses compiled in Carn et al. (2016). The detection of SO<sub>2</sub> degassing from October 1978 to September 2004 was generally restricted to TOMS measurements, which only captured degassing events from large explosive eruptions. IASI data were also used to quantify active emissions after 2006 (Carn et al., 2016; Theys et al., 2013). In September 2004 OMI became fully operational, and, with an increased spectral resolution and smaller footprint size, it provided a previously unseen level of SO<sub>2</sub> sensitivity (Carn et al., 2016). OMI is currently in operation and is capable of detecting explosive/high-altitude degassing from smaller eruptions than its predecessors, as well as passive/low altitude volcanic SO<sub>2</sub> emissions (Carn et al., 2008). Where detectable, annual mean passive SO<sub>2</sub> emissions from Carn et al. (2017) are included in the degassing data set. In Figure 2b, active degassing measurements are presented in the plots as a single discrete point, while mean annual passive degassing measurements are shown as a bar spanning the year where the measurements were made. In some cases, the emissions from one volcano were impossible to differentiate from those of a neighboring

volcano. Where this occurs the combined emissions for both the volcanoes are included in the degassing data set, and this combined measurement is noted in the figure caption.

### 2.3. Thermal

Thermal infrared and middle infrared instruments like ASTER on the Terra satellite (launched in 1999) and MODIS (Table 1) on the Terra, as well as the Aqua satellite (launched in 2002), have been utilized to detect volcanic thermal anomalies (Dehn et al., 2002; Francis & Rothery, 1987; Kaneko & Wooster, 1999; Oppenheimer & Francis, 1997; Oppenheimer et al., 1993). Although both sensors provide spectral radiance values from which thermal flux and other metrics can be derived, the different spatial and temporal resolutions of these sensors provide different sensitivities to volcanic activity. The ASTER sensor has a spatial resolution of 90 m in the thermal infrared spectrum and a temporal resolution that is limited to 1–7 days in the polar regions and 16 days at the equator (a cross-track pointing mirror can, in important cases, reduce this repeat time; Ramsey, 2016; Yamaguchi et al., 1998). These data are sensitive to smaller changes in thermal output than the MODIS sensor, but the low temporal resolution in areas with persistent clouds can result in sparsely populated time series.

ASTER temperature data used in our time series were collected as part of the ASTER Volcano Thermal Output Database (AVTOD) project and are presented as temperature above background (Figure 2c). This database uses the kinetic surface temperature (AST\_08) data product (Gillespie et al., 1998) and improves upon methods from Jay et al. (2013) and Reath et al. (2016). Temperatures above background were determined by calculating the average temperature of a 10-by-10-pixel region adjacent to the thermal anomaly and subtracting that from the maximum pixel temperature of the anomaly. In cases where the pixel temperature was saturated, a temperature of 120 °C was assigned. This corresponds with the approximate temperature of saturation in the ASTER brightness temperature algorithm (Abrams et al., 2002). All available cloud-free ASTER nighttime acquisitions are included in this data set, meaning zero values are included. We define an image to have clouds if atmospheric water vapor covers the anomalous area or if clouds are in close proximity to an apparent anomaly and appear to have an influence on its temperature, based on the discretion of the investigator.

Two MODIS-based volcano thermal archives are incorporated into the thermal data set used here: MODVOLC (Wright, Flynn, et al., 2004) and MIROVA (Coppola et al., 2016). MODIS data are collected twice daily, resulting in a much more complete time series of observations compared to ASTER, but with a spatial resolution of 1 km, resulting in a higher detection threshold for thermal outputs than ASTER. The majority of the MODVOLC data we used come in the form of detected alerts, which are triggered whenever a thermal anomaly produces a thermal signature that exceeds the normalized thermal index (NTI) volcanic activity threshold (Wright, Flynn, et al., 2004). This threshold is designed to limit false triggers; however, it also limits MODVOLC's ability to trigger alerts for volcanic anomalies that produce a low thermal output. These alerts are therefore focused on large thermal events such as active eruptions and lava flows (Wright, Flynn, et al., 2004). At particularly active volcanoes, enough MODVOLC alerts have been triggered that the trend of detected thermal energy can be plotted in J/month (Wright, 2016). Where applicable, these trends have been included in the thermal plot as a bar spanning the month where increased thermal energy was detected. However, in all but two of these cases volcanic radiative power data from MIROVA are also available, and, due to the increased accuracy of these measurements, they replace the MODVOLC (J/month) trend in the thermal plots. Volcanic radiative power measurements have increased accuracy due to the more complex MIROVA algorithm, which incorporates both spatial and spectral filtering and provides increased sensitivity to thermal anomalies with lower thermal outputs (Coppola, et al., 2016). These data are provided in Watts and are included in the plots as a single yellow dot (Figure 2c). The MIROVA system is relatively new, and previously acquired MODIS data are still being processed; therefore, measurements for some volcanoes of interest in this study are not currently available.

### 2.4. Deformation

InSAR is used to detect ground deformation that arises from a variety of volcanic processes (e.g., Chaussard & Amelung, 2014; Lu et al., 2010; Pinel et al., 2014; Pritchard & Simons, 2004). Compared to the degassing and thermal data sets, the deformation data included here are much more heterogeneous with respect to satellite source (15 sensors used) and analysis methods (Table 1). For example, ENVISAT had seven different

acquisition modes, two of which are included in this study, Image Swath (IS)-2 (23° look angle), which was used in the nominal mission from March 2002 to October 2010, and IS-6 (45° look angle), primarily used in the extension mission from October 2010 to April 2012. Each of these acquisition modes is sensitive to different components of deformation (e.g., Kouamé et al., 2006), restricting the data from being plotted as a continuous time series. ALOS-1/2 is also unique in that they use the L-band (~24 cm) wavelength, which penetrates some vegetation (e.g., Lucas et al., 2010). Due to this characteristic, many heavily vegetated volcanoes only have deformation data from ALOS-1/2. Based upon the amount of deformation data available for each volcano of interest, some combinations of data from each of these instruments have been used to create each deformation time series plot (e.g., Berardino et al., 2002). Automated systems for processing SAR data are not yet operational (although see Hua et al., 2013; Meyer et al., 2016; Spaans et al., 2017); therefore, all the deformation data included in these plots are from previous publications, as cited in the figure captions, or the result of new work. The specific instruments used are always noted, and when multiple acquisition modes or frames are used from the same instrument, they are plotted separately (Figure 2d). Where possible, the location of measured deformation and the timing of the zero displacement reference acquisition have been included in Table S2.

To facilitate interpretation of the deformation data sets, different markings are used to indicate the type of method (Text S1) utilized to analyze the data. For example, a closed mark is indicative of the true measurement of displacement as determined from the sensor data, although these values may include atmospheric and spatial filtering corrections. An open mark is indicative of interpolated data—Each mark represents the data acquisition times, but the displacement values are interpolated from the general trend of displacement of these acquisitions. These trends are determined either from literature or from individual interferograms. There are also sections of the plot with a light blue background, indicating periods with no ground displacement above uncertainty. Error has not been calculated for every available deformation time series; therefore, error bars are not included in these plots. Time series with previously calculated error values can be found in Table S3.

### 3. Results

Time series figures depicting ground-based observations as well as coincident satellite observations of gas emissions, thermal anomalies, and deformation for 47 volcanoes are included in this study as Figures S1–S47. Because a discussion of each volcano's figure is impractical, we summarize general trends and highlight a few examples to illustrate the utility and challenges of using satellite observations to detect volcanic unrest and characterize volcano behavior.

#### 3.1. Comparison of Unrest and Eruption Time Series: Copahue Volcano

We have performed an in-depth study of Copahue volcano, located on the Chile–Argentina border to demonstrate how complementary data types can be used together (Figure 2). Since its 2000 eruption, Copahue has been the subject of numerous ground-based studies aimed at characterizing baseline behavior (e.g., Agosto et al., 2013; Caselli et al., 2005; Ibáñez et al., 2008). Our analyses expands upon previous studies (e.g., Carn et al., 2017; Lundgren et al., 2017; Velez et al., 2011, 2016), through inclusion of new thermal time series data and filling gaps in the deformation time series from 2008 to 2011.

At Copahue, local monitoring presented by BGVP (Figure 2a) reveals two periods of activity. The first period in early- to mid-2000 corresponds with an eruptive event that lasted from 1 July to 18 October 2000 (maximum VEI of 2). A wide range of ground-based detections were made, in contrast to the very limited satellite detections during that time (Caselli, Velez, et al., 2016; Naranjo & Polanco, 2004; Varekamp et al., 2001). After this eruption, no new activity was detected until early 2012, when phreatomagmatic eruptions occurred and intense bubbling of the crater lake leads to its complete evaporation (Caselli, Agosto, et al., 2016). These signals heralded the onset of a new explosive eruptive phase that was categorized by GVP as occurring from 22 December 2012 to 10 December 2013. After this eruptive period, regular observations revealed seismic, ash, gas, thermal, and explosive activity as Copahue continued to demonstrate cyclical behavior of eruption and inactivity for the remainder of the study.

The degassing time series (Figure 2b) shows temporal variations in passive degassing as well as active degassing from the largest eruption during the observation period. We observed no evidence of active degassing



in TOMS sensor data during the 2000 eruption. In 2005, when OMI data became available, passive degassing was episodically detected, in low quantity ( $<45$  kt/year) until 2012. Passive degassing increased significantly in 2012 and reached its peak in 2013. A large active degassing event on 22 December 2012 corresponded with the emission of a large ash plume that led to the alert level of the volcano to be raised from orange to red by the Observatorio Volcanológico de los Andes del Sur-Servicio Nacional de Geología y Minería (Venzke, 2013).

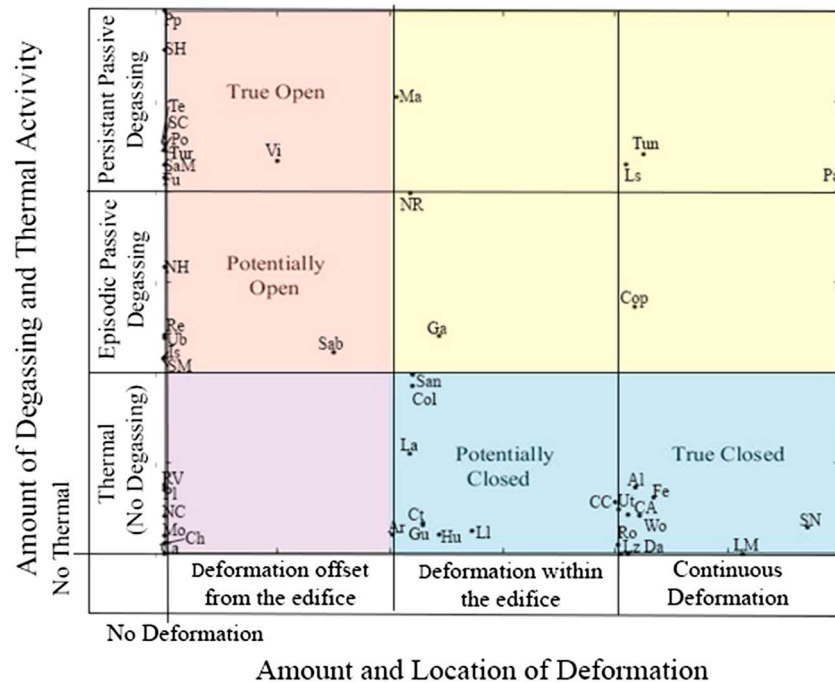
The thermal output (Figure 2c) reveals several different trends that we relate to eruptions, removal of the crater lake, and fumarolic activity. After 21 November 2009, temperature variability increased in the ASTER data, leading to a trend of increasing temperature in both ASTER and MIROVA data types, between 5 September 2012 and 16 July 2012. When this trend reached its maximum on 16 July 2012, observers on the ground reported intense bubbling of the crater lake and phreatomagmatic eruptions (Caselli, Agosto, et al., 2016; Venzke, 2013). Based on our observations we speculate that during this period, the crater lake began to evaporate or was erupted away at a faster rate than it could refill. Removal of the crater lake produced lower thermal readings for both ASTER and MIROVA by both removing a surficial element storing heat and by reducing the area of the thermal anomaly from the full crater lake to that of a few hot fumaroles. This was observed through analysis of ASTER data, which demonstrates that the anomaly detected on 19 October 2012 decreased in both area and intensity compared to the anomaly detected 24 July 2012 (Figure S48), suggesting the partial or complete evaporation of the lake within this period. For the remainder of the study Copahue underwent several eruptive cycles, and thermal output was highly variable and seemingly cyclical, with temperatures varying as much as  $0.92$  °C/day (25 October to 26 November 2014), and the highest values were recorded at the conclusion of explosive activity during the three separate eruptive periods.

Ground deformation at Copahue determined from multiple satellites (Figure 2d) demonstrated a long-term trend in subsidence and then a change to uplift. The deformation data set begins on 16 December 2002 with a consistent deflation trend of  $\sim 2$  cm/year (LOS) in both Envisat IS-2 (Velez et al., 2016) and ALOS-1 data until 26 March 2010, where a transient spike in the deflation (circled in Figure 3d) is seen that we suggest may be related to the 2010 Maule earthquake, similar to subsidence at five other volcanic systems in southern Chile (Pritchard et al., 2013). After the 2010 subsidence event, deflation transitioned to inflation, which was first observed by the 27 December 2010 acquisition (Velez et al., 2016). The correlation between the timing of the deformation transition and the Maule earthquake provides evidence supporting the theory of Bonali (2013) that earthquake-induced stress played a role in retriggering activity in the Copahue volcanic system. After the transition to uplift, inflation continued at an initial rate of 12–15 cm/year before exponentially decreasing over time (Lundgren et al., 2017). Velez et al. (2016) proposed that during the 10-year deflation period, subsidence was related to degassing of the hydrothermal system, while the inflation since 2012 was due to pressurization of a deeper magmatic source. The inflation persisted through several eruptive cycles (Figure 2d; Lundgren et al., 2017; Velez et al., 2016).

By comparing the different subpanels in Figure 2, it becomes evident that the near synchronous timing of certain events and changes in observed trends could suggest common source processes. In all four data sets the level of activity is limited between late 2000 and early 2010. In 2011, an inflation trend begins at about the same time as an upward trend in thermal output. Notably, these trends are observed in satellite data before complementary ground observations were reported in BGVP, with the first ground reports starting in early 2012 and unrest in all three satellite parameters starting in early- to mid-2011. If new magma was introduced into a shallow reservoir (e.g., Velez et al., 2016), it could have triggered the change from subsidence to uplift and also provide heat to the fumaroles and the crater lake. In 2012, thermal output became variable, and the rate of passive  $\text{SO}_2$  degassing increased. Both observations are consistent with the removal of the crater lake during the July and December 2012 phreatomagmatic eruptions, after which time the lake was not present to provide a higher and more consistent anomaly temperature nor to scrub  $\text{SO}_2$  gas. From 2014 to the end of the observation period, higher temperatures with increased cyclical variability and slightly lower, but still elevated passive degassing rates, are recorded.

### 3.2. Open and Closed Volcanic System Classifications

Our compilation of satellite data at 47 different volcanoes allows us both to compare how manifestations of volcanic unrest relate to eruptions and to test conceptual models of open and closed conduit volcanoes.



**Figure 3.** Classification of the 47 study volcanoes in Latin America based on the amount of degassing/thermal output produced compared against the amount of deformation. Volcano names were abbreviated as Al = Alcedo, Ar = Arenal, Ca = Calbuco, CA = Cerro Azul, Ch = Chaitén, NC = Nevados de Chillán, Col = Colima, Cop = Copahue, CC = Cordón Caulle, Ct = Cotopaxi, Da = Darwin, Fe = Fernandina, Fu = Fuego, Ga = Galeras, Gu = Guagua Pinchincha, Hu = Hudson, NH = Nevados del Huila, Is = Isluga, La = Láscar, Ls = Lastarria, Lz = Lazufre, Ll = Llaima, Ma = Masaya, LM = Laguna del Maule, Mo = Momotombo, Pa = Pacaya, PI = Planchón-Peteroa, Po = Poas, Pp = Popocatepetl, Re = Reventador, RV = Rincon de la Vieja, Ro = Robledo, NR = Nevado del Ruiz, Sab = Sabancaya, SC = San Cristóbal, SM = San Miguel, San = Sangay, SaM = Santa María, SN = Sierra Negra, SH = Soufrière Hills, Te = Telica, Tun = Tungurahua, Tur = Turrialba, Ub = Ubinas, Ut = Uturuncu, Vi = Villarrica, and Wo = Wolf.

Several definitions exist in literature for open and closed volcanic systems. The classification of Newhall (2007), which we refer to as the “degassing definition,” focuses primarily on gas emissions—Open volcanic systems passively degas any exsolved volatiles from the magma body due to a permeable conduit that allows these gases to escape the system. In a closed system, these exsolved gases cannot separate from their host magma due to a high magma viscosity or impermeable conduit (Text S2). Chaussard et al. (2013) define open and closed systems based on their characteristics of surface deformation, and we refer to this as the “deformation definition.” In an open system, when gases or pressure from an influx of magma enters the system, pressure is relieved in a short time span through the open conduit without significant observable surficial deformation. The opposite is true of closed systems, where detectable deformation is common. Both of these studies rely on measuring different types of unrest but are related. Passive degassing pairs with a lack of deformation within open systems and the opposite should hold true for closed systems. While these classifications facilitate the understanding of particular aspects of volcanic systems, they may not apply to all dynamic volcanic systems.

In order to explore the practicality of using this classification system, all 47 volcanoes included in the study have been categorized in the context of these classification definitions using the remote sensing observations of deformation, degassing, and thermal data (Figure 3 and Table S4). The y-axis of Figure 3 shows the relative degassing from each volcano, as the amount of passive SO<sub>2</sub> emissions (where such measurements exist) and/or observed thermal output as a proxy for fumarolic activity where degassing data do not exist. The reasoning behind including both thermal and degassing observations on the same axis is that a lack of detected passive SO<sub>2</sub> emissions does not necessarily mean the volcano is not degassing. The emissions may just be below the detection threshold for the OMI sensor (Carn et al., 2013), and/or the gas composition is dominated by other gases (CO<sub>2</sub>, H<sub>2</sub>O, and H<sub>2</sub>S). Thermal readings can act as an expression of passive

degassing where hot magmatic gases provide heat to the surface producing a thermal anomaly. Additionally, even if these thermal anomalies are not directly related to hot gases, but to the rise of heat from the magma body, the ability of the heat to reach the surface at a single persistent location likely indicates a semipermeable conduit. The  $x$ -axis of Figure 3 demonstrates the rate and location of measured ground deformation by InSAR. Limitations inherent in each of these data types may have a nonuniform effect on average values and detection limits based on the amount of data available and surrounding vegetation at these volcanoes; these limitations are discussed further in section 4.1.

Each axis has three separate subintervals to represent three categories of activity observed at these volcanoes (listed from high values to low values), including persistent degassing, episodic degassing, and thermal signature with no measured degassing on the degassing/thermal axis ( $y$ -axis) and continuous deformation, deformation within the edifice, and deformation offset from the edifice (see rationale in Text S4) on the deformation axis ( $x$ -axis). Values within these subintervals are calculated using different gauges; both persistent and episodic passive degassing category values are determined through calculating the average annual  $\text{SO}_2$  emissions from 2005 to 2015, limited to data collected from the OMI sensor. Thermal values are determined from the average temperature above background values determined from ASTER data during non-eruptive periods of the entire time series (2000–2017). This includes thermal readings derived from the hottest volcanic vent during pre-eruptive and post-eruptive periods. All numeric values are shown in Table S4.

Deformation values are the *absolute value* of the amount of deformation (e.g., 3 cm of deflation followed by 6 cm of inflation would be measured as 9-cm total deformation). Deformation occurring during an eruptive period is not included in the total deformation value; further explanation of how these values are calculated is provided in S3. In the continuous-deformation category values in Figure 3 and Table S4 are determined by the monthly average deformation rate for the full time series, whereas in both the deformation within the edifice and offset from the edifice (explained in S4) categories, values are determined by the amount of deformation measured 6 months before eruption onset as classified by the GVP. In the latter two categories, measurements were limited to a 6-month period due to the transient nature of the deformation that frequently occurs before an eruption. In this study, deformation activity was often detectable for at least a 6-month period at the erupting volcanoes.

For each volcano, we have applied the following rules in making Figure 3. The timing of each eruptive period is determined by the values provided by the GVP, and the mechanics of this timing is discussed in section 2.1. Only eruptions with a VEI values of 1 or greater are considered for this study. The scale for each of these categories in Figure 3 has been normalized so that the highest value is at the top (or right) of the axis whereas zero represents the lowest value. We term unrest as “transient” if, at any point during this study, no unrest can be detected. Volcanoes with no detectable deformation and/or thermal anomalies for the full study plot at the zero lines of each of these axes.

In Figure 3, we use a color code for the different types of volcanic systems. The region shaded pink in the plot fulfills the expected unrest of an open system and the blue region that of a closed system, as established by both the degassing and deformation definitions. Volcanoes falling in to the yellow region produce both passive degassing and surficial deformation and would be classified as *open* using the degassing definition and *closed* using the deformation definition. Conversely, volcanoes in the purple region provided little to no remotely detectable unrest. These volcanoes would be classified as *closed* by the degassing definition and *open* by the deformation definition. These color codes only apply to unrest detected from 2000 to 2017—During other time periods the volcano behavior may differ.

If every volcano fit neatly into the open and closed definitions, before eruptions we would see open systems degassing without deformation and closed systems without degassing, but with deformation. While this simple open or closed behavior is seen at a majority of the volcanoes (mentioned below), many do not fit neatly into these two categories but are a combination of the two (Figure 3). Of the 47 volcanoes studied, 19 exhibited the typical behavior expected in a closed system, and 15 exhibited that of an open system. Seven volcanoes exhibited both passive degassing and clear deformation in the pre-eruptive period, and six volcanoes had little to no detectable pre-eruptive unrest in either category. In both of these cases, the volcano could be classified as either open or closed, dependent upon whether the degassing or deformation definition was being used. To further complicate this issue, volcanoes are dynamic systems. In closed systems with magma reservoirs at depth, compressible magma and/or ductile wall rocks can deform to accommodate

the influx of new magma without transmitting a deformation signal to the surface (Anderson & Segall, 2011). Further, eruptions can force open conduits in a closed system and collapse conduits in an open system, changing the system behavior, and thus our classification after eruption.

Whereas these classifications oversimplify a complicated issue, this study has identified some volcanoes that seem to fit closely to the open and closed system definitions. Villarrica volcano presents a classic example of an open conduit volcanic system (Figure S46). Villarrica is characterized by a ~40-m-diameter lava lake that varies from 20 to 100 m below the crater rim (e.g., Moussallam et al., 2016; Shinohara & Witter, 2005). Passive degassing is consistently above detectable limits, and variations in the annual emission rates correlate closely with thermal measurements for the period of study. These cycles of increased and decreased thermal and degassing output are closely related to periods where the lava lake is or is not present, acting as a reliable proxy of magma levels within the conduit. All exsolved gases and pressure from the influx of new magma to the shallow reservoir are able to escape the open system from the conduit, causing a change in the level of the lava lake before building up enough pressure to cause remotely detectable deformation. Delgado et al. (2017) determined deformation relating to activity at Villarrica could be detected in the SE edifice flank from mid-April to mid-May 2015 (after the March 2015 eruption) but did not detect deformation on the volcanic edifice or anywhere else before the 2015 eruption.

In a closed system, overpressure builds in the magma reservoir, whether from the influx of new magma or volatile exsolution, causing inflation. In many cases, the pressure of the reservoir exceeds the tensile strength of the surrounding rock, opening a conduit that leads to an eruption (e.g., Chaussard et al., 2013). Wolf volcano (Galapagos Islands, Ecuador) presents a classic example of a closed volcanic system (Figure S47). Wolf is an active shield volcano that demonstrates a cyclical behavior of caldera collapse with partial caldera refill between eruptive phases (e.g., Geist et al., 2005). In this system, the volcano is continuously inflating during noneruptive periods, and no passive degassing can be detected. A thermal signature, while low relative to the other volcanoes in our study area, is detectable with ASTER during noneruptive periods. In this closed system, a very limited amount of volatiles and pressure are discharged through the conduit, resulting in enough subsurface pressure buildup for deformation to be expressed on the surface as consistent inflation as well as a thermal anomaly.

Both Villarrica and Wolf provide good end-members to demonstrate the utility of the open and closed classification system, although in each of these cases attributes of the opposing system type are observed. Deformation offset from the edifice has been identified at Villarrica by Delgado et al. (2017) and a persistent thermal anomaly ~10 °C above background has been detected at Wolf (Figure S47). In fact, a majority of volcanoes produce some attributes associated with both classifications. Copahue is an example of such a volcano (Figure 2). Before the 22 December 2012 eruptive cycle, pre-eruptive behavior was observed using all three techniques. Although this system does have a permeable conduit that enables passive degassing, it must be constricted (Bruce & Huppert, 1989) to a degree that it cannot relieve subsurface pressure as quickly as it builds (Girona et al., 2015). This forces the magma reservoir to inflate in response to the excess pressure, thus producing detectable deformation. In such a system, the volcano would exhibit deformation behavior similar to a “closed” system despite having an “open” conduit.

There are also cases where volcanoes erupt with seemingly no pre-eruptive unrest, such as Chaitén, which exhibited neither degassing nor deformation before its 2 May 2008 VEI 5 eruptive event (Figure S5). In fact, the only detectable pre-eruptive unrest manifested as an increase in seismicity 1 day before the eruption (Wunderman, 2008). However, this volcano was not well monitored, with the closest seismometers several hundred kilometers away. No measurable unrest was detected by any of the remote sensing techniques. It is theorized that this eruption was caused by magma from a deep source, located well to the east associated with Minchinmavida volcano, that rapidly ascended through existing faults (e.g., Wicks et al., 2011). This system is characterized as a closed system; however, we speculate that the magma source is deep enough that any pre-eruptive deformation in the magma reservoir was not expressed on the surface. After the eruption, the thermal baseline increased due to a newly emplaced and actively effusing lava dome, indicative of an open system and demonstrating the temporally dynamic nature of volcanic systems. If eruptive activity occurs while the volcano is in an open state, it would likely be preceded by both an increase in thermal and degassing output.

Along with Chaitén, five other volcanoes in this study demonstrated similar pre-eruptive characteristics: Calbuco, Nevados de Chillán, Momotombo, Planchón-Peteroa, and Rincon de la Vieja. Although of these six volcanoes, only Chaitén and Calbuco truly lack any type of satellite detectable pre-eruptive unrest. Measureable thermal unrest was detected at all other volcanoes, suggesting some form of open conduit. Additionally, no deformation data are available for Rincon de la Vieja, and limited deformation data are available for Momotombo and Planchón-Peteroa. In these cases, a lack of detectable unrest may be due to the limited availability of data, rather than volcanic characteristics.

Observed variations in the established classification scheme of open and closed systems demonstrate how volcanoes cannot be simply categorized. Rather, the concepts of open and closed volcanoes should act as endpoints for the dynamic possibilities of volcanic systems. As we demonstrate here, there exists a range of volcanoes that fall outside of these classifications and volcanoes that are capable of transitioning between end-member states. Additionally, volcanoes that most closely match the ideal open and closed systems commonly contain some aspects of the other system.

## 4. Discussion

### 4.1. Limitations of Satellite Volcano Monitoring

The amount and type of satellite data available greatly impact the effectiveness of remote sensing for volcano monitoring, and it is common for volcanic activity to be missed because of poor spatial, spectral, or temporal resolution of the available data types (e.g., Carn et al., 2016; Moran et al., 2006; Pieri & Abrams, 2005). Each data type has different characteristics affecting the availability and quality of data.

SO<sub>2</sub> degassing data are continuously available from 2004 to present as part of the NASA Global Sulfur Dioxide Monitoring home page. However, they are limited by the 13 × 24 km pixel size, masking from anthropogenic SO<sub>2</sub> sources (e.g., Mexico City masks Colima), and atmospheric conditions. Additionally, passive degassing in all but the most extreme cases was undetectable with moderate spatial resolution instruments until the OMI sensor began operation in 2005. Further, UV sensors such as OMI only operate by day, and their detection limits vary as a function of altitude, latitude, and season (e.g., Carn et al., 2003).

Thermal data are masked by cloudy conditions, which can be particularly problematic in forested tropical areas, and high spatial/ low temporal resolution data can have significant data gaps. A study performed as part of AVTOD found that only ~22% of ASTER scenes acquired for volcanoes in this study in Central America and the North Andes were cloud free enough to be usable, compared to ~60% of scenes in the Central Andes (Table S5). In addition, ASTER data are not continuously acquired and, in the case of AVTOD, are limited to nighttime acquisitions. MODIS data for the entire time period of 2000–2017 are analyzed by MODVOLC, but the MIROVA database is still relatively new, and the entire MODIS archive from every volcano included in this study has not yet been processed.

SAR data, used to determine deformation, have the benefit of providing ground information through clouds but are affected by tropospheric water vapor and surface decorrelation in heavily vegetated areas (e.g., Ebmeier et al., 2013a, 2013ab). Certain observation modes (using longer radar wavelengths or higher spatial resolution at a given wavelength) improve coherence in vegetated areas, but these data are not always available at no cost. The benefits of these modes for Latin American volcanoes and their utility for monitoring are described in Pritchard et al. (2018).

Table 2 acts as quick guide for the availability of SAR and certain types of thermal data for all 47 volcanoes and identifies if the volcano has had an eruption (Y/N) during the period of study. Degassing data are not included in this plot because OMI data are continuously monitored for SO<sub>2</sub>, since 2005—therefore, the current maximum level of coverage is already available, although the detection threshold varies with location (e.g., Carn et al., 2013). For simplicity, we consider all volcanoes to have the same availability of degassing data. Likewise, the MODVOLC algorithm has consistently been applied to every volcano on this list on a twice-daily basis, although MODVOLC alerts are generally limited to eruptive events. Data sets with increased sensitivity to subtler thermal anomalies, like ASTER and MIROVA, are necessary to detect thermal activity occurring in noneruptive periods. Thus, the analysis of thermal data availability is limited to the cloud-free nighttime ASTER (i.e., AVTOD) and MIROVA data types. We define high thermal data availability as having an average of over 10 AVTOD detections per year and/or the MIROVA data set has no gaps longer than 2 years. We

**Table 2**  
Data Quality Table of 47 Volcanoes with Time Series, Green(3) = High Data Availability, Yellow(2) = Intermediate, and Red(1) = Poor

Volcano	Eruption	Thermal	Deformation
Alcedo	N	3	3
Arenal	Y	2	1
Calbuco	Y	3	2
Cerro Azul	Y	3	3
Chaitén	Y	3	3
Nevados De Chillán	Y	3	3
Colima	Y	3	3
Copahue	Y	3	3
Cordón Caulle	Y	2	3
Cotopaxi	Y	2	2
Darwin	N	3	3
Fernandina	Y	2	3
Fuego	Y	3	2
Galeras	Y	2	2
Guagua Pichincha	Y	1	2
Hudson	Y	2	2
Nevados del Huila	Y	2	2
Isluga	N	3	2
Láscar	Y	3	3
Lastarria	N	3	2
Lazufre	N	3	3
Llaima	Y	3	3
Masaya	Y	3	2
Laguna del Maule	N	3	3
Momotombo	Y	3	2
Pacaya	Y	3	2
Planchón-Peteroa	Y	3	2
Poas	Y	2	2
Popocatepetl	Y	3	2
Reventador	Y	3	2
Rincon de la Vieja	Y	1	1
Robledo	N	1	2
Nevado de Ruiz	Y	2	2
Sabancaya	Y	3	3
San Cristobal	Y	2	2
San Miguel	Y	1	2
Sangay	Y	3	1
Santa María	Y	3	1
Sierra Negra	Y	1	3
Soufrière Hills	Y	3	1
Telica	Y	2	2
Tungurahua	Y	3	2
Turrialba	Y	2	1
Ubinas	Y	2	2
Uturuncu	N	2	3
Villarrica	Y	3	3
Wolf	Y	2	3

define intermediate data availability as having at least one AVTOD measurement per year and/or any MIROVA detections, and poor data availability as having less than one AVTOD measurement per year. For the deformation data, the data availability is considered high if some form of deformation time series data is available for 10 of the 17 years of this study, intermediate data availability if there is less than 10 years of deformation time series data, and poor data availability when there is no deformation data.

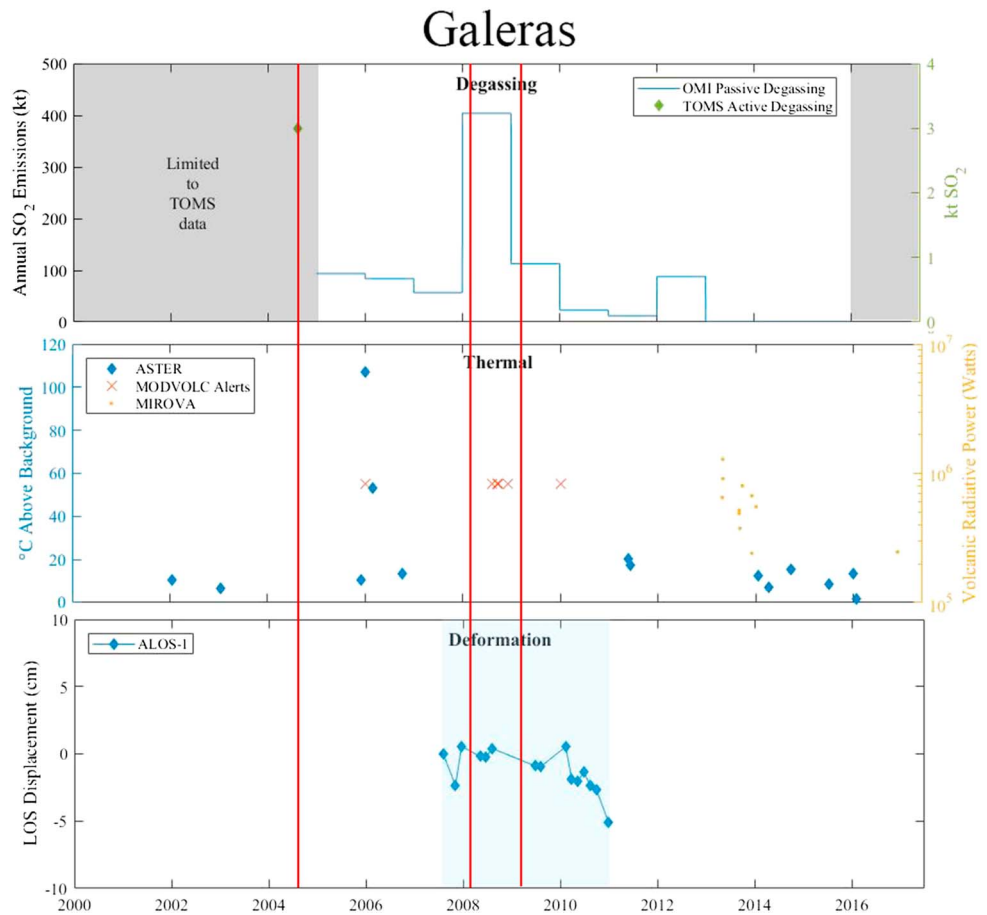
The availability of data can have a large effect on the ability to make meaningful interpretations. Using Figure 3 as an example, although all values used are averaged over a 17-year period, a lack of data available can lead to the overemphasis or underemphasis of short-term thermal and degassing activity in this average, depending on when the data are acquired. This issue can be exaggerated in low temporal resolution (i.e., ASTER) data where values are, in some cases, determined from less than 20 acquisitions. Further, in highly vegetated areas, subtler surface deformation is more difficult to detect, potentially biasing the data toward open systems in these locations. Additionally, without the proper amount of data to establish a new trend in volcanic unrest, it becomes unrealistic to determine volcanic characteristics with satellite sources. Table 2 identifies the variations in the availability of the satellite data for each volcano, in order to determine where potential gaps in data coverage may exist. Our simplistic criteria for data availability do not provide an overview of the data quality, only quantity. A qualitative metric would require a more comprehensive analysis and is recommended for future work.

#### 4.2. Pre-Eruptive Trend Identification

An obvious question is whether the satellite data provide any indication of impending eruption. Here we have performed a qualitative analysis of where the most common types of pre-eruptive trends are observed in these data sets before some of the largest eruptions. A complete analysis of the pre-eruptive trends in each of these time series would require a statistical analysis of the noneruptive period of each volcano to determine the threshold of noneruptive variation and is beyond the scope of this work.

During our study period, 20 eruptions at 14 volcanoes were classified as having either VEI 3, 4, or 5 eruptions (Venzke, 2013). Using the satellite time series for these volcanoes, we have identified whether a change in satellite-detected unrest was observed before these eruptions (Table S6). Specifically, we looked for characteristics that could be classified as a pre-eruptive trend, including (1) inflation or an increase in inflation rate in deformation data, (2) increases in thermal output, and (3) an increase in SO<sub>2</sub> emissions. Future work will investigate whether an approach of relying on these features alone is overly simplistic or if the inclusion of more complex parameterizations is more appropriate.

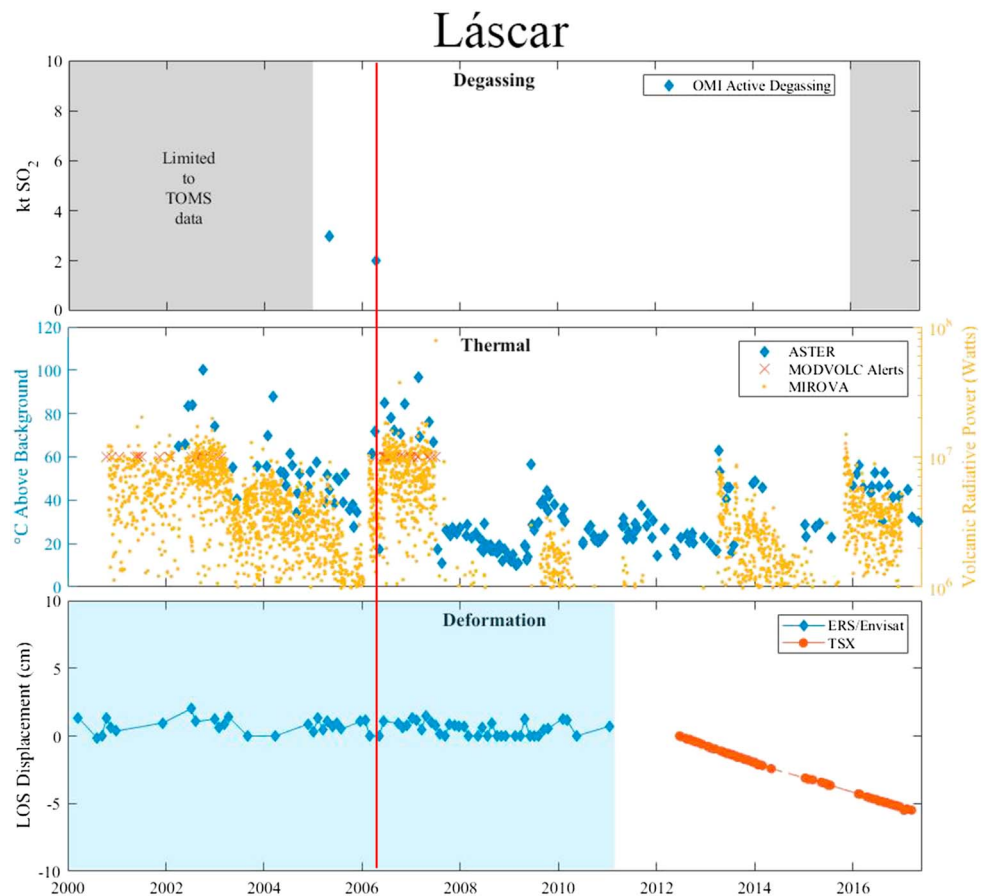
In this analysis, pre-eruptive changes in the trend were evident at fewer volcanoes than expected. Only one eruption at Sabancaya (Figure S33) had a pre-eruptive change in trend from all three data types (Table S5), and only the Nevado del Ruiz (Figure S34) eruption had two types of identifiable pre-eruptive changes in trend (Carn et al., 2017; Lundgren et al., 2015). Nine eruptions had one type of identifiable change in trend, and the final nine eruptions produced no easily identifiable pre-eruptive trends. Though the number of volcanoes with a pre-eruptive trend is



**Figure 4.** Satellite time series for Galeras volcano, Colombia. See Figure 2 caption for details about symbols. Deformation data provided by (a). Morales from the point 1.2275,  $-77.3486$  (Morales Rivera et al., 2016) these data have high uncertainties due primarily to the variability of atmospheric water vapor in tropical regions (Ebmeier et al., 2013a, 2013b). Red lines have been added to this figure to signify the timing of three VEI 3 eruptions.

low, there are a number of factors that smitigated the likelihood of detection. First is the simplicity of this inspection. We are only looking for the most common types of trends; however, previous literature (Biggs & Pritchard, 2017; Reath et al., 2016) has identified multiple other types of trends that are not being accounted for in the study. Second, without a quantitative analysis, a qualitative inspection identifies these trends with a limited degree of accuracy. Third, data limitations reduce the ability of the observer to identify where pre-eruptive trends occur. This can be a significant limitation, as ground-based changes in unrest that are diagnostic of coming eruptions often take place only days to hour preceding an eruption (e.g., Mothes et al., 2015; Wadge & Aspinall, 2014; Wadge et al., 2014). In these cases, the unavailability of near-real time data or infrequent satellite acquisitions can pose a serious issue.

Galeras volcano (Figure 4) provides an example of how data limitations can lead to an unclear perception of pre-eruptive trends. Three VEI 3 eruptions were recorded at Galeras during our study period. Before the 16 July 2004 eruption of Galeras, OMI had not been launched, so any passive degassing would have been undetectable, no deformation data were available due to the lack of a sensor with coherent observations given the dense vegetation, and no ASTER scenes had been acquired for over 2 years. Although a lack of ground-based reports makes it unclear if a pre-eruptive trend would have been detected, this is a case where a lack of data eliminates any possibility of pre-eruptive evidence. Both degassing and deformation data are available before the 17 January 2008 eruption; however, it is unclear if the measurements made by these techniques can be related to a pre-eruptive change in trend. This is because there is a singular point of increased negative displacement before the event (Parks et al., 2011); however, the variations in these data are below the



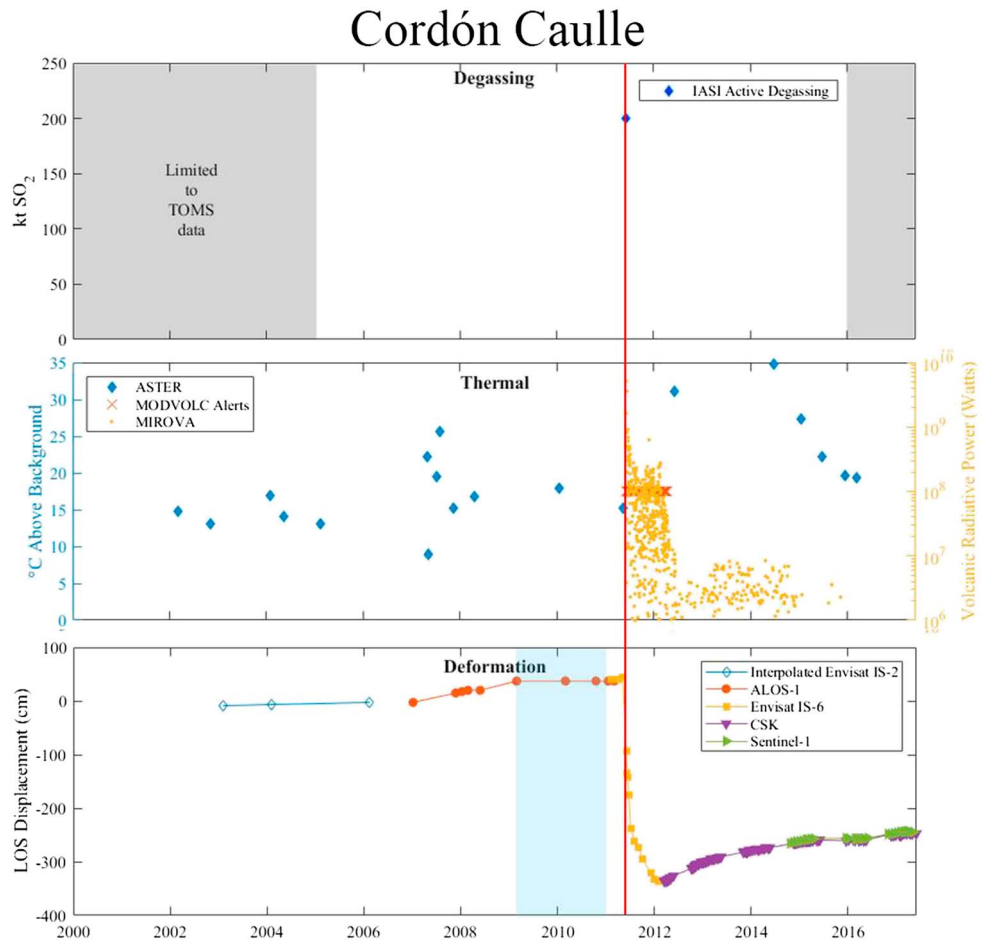
**Figure 5.** Satellite time series for Láscar volcano, Chile. See Figure 2 caption for details about symbols. TSX deformation data provided by N. Richter from the point  $-23.363, -67.726$  within the crater from (Richter et al., 2018). From 04 May 2014 to 12 Jan 2015 there is a time series data gap; displacement during this time has been interpolated to be consistent with displacement of both sides of the gap. The combined ERS/Envisat time series from the point  $-23.37, -67.73$  (S. T. Henderson & Pritchard, 2013) does not show any consistent deformation, but because the ERS/Envisat InSAR data was processed at much lower resolution, it could have missed the deformation detected by TSX during the later time period. The light blue area of the deformation graph marks the time over which the rate of any magmatic deformation is below the measurement threshold; any measured variability is believed to be the result of atmospheric interference. The vertical red line signifies the timing of the 18 April 2006 VEI 3 eruption.

threshold for atmospheric noise. Whereas there is an increase in passive degassing in the same year as this eruption, it is unclear if this increase occurred during the pre-eruptive period of this eruption, before the next eruption or even during the eruption. Once again, no thermal data were acquired for over a year before eruption.

Very similar issues affect the pre-eruptive data before the 14 February 2009 Galeras eruption; (a) the eruption occurs too soon after the previous eruption to determine if there is a pre-eruptive increase in degassing, (b) noise levels and data gaps make the deformation data unclear, and (c) a lack of ASTER data provide limited thermal readings. MODVOLC did trigger some alerts during the pre-eruptive period; however, it is unclear how these relate to the upcoming eruption and MIROVA data are unavailable, as they have only been processed up to 2013 for this volcano.

Conversely, at some volcanoes with a dense satellite data set, pre-eruptive trends were identified. For example, a subtle and temporally limited increase in thermal output was measured by ASTER before the 18 April 2006 eruption at Láscar (Figure 5), where ASTER data were acquired 12 days before eruption. Similarly, at Cordón Caille (Figure 6) a possible subtle increase in inflation rate associated with seismicity potentially caused by a transient magma injection leading to the 4 June 2011 eruption as measured in Envisat IS-6 data acquired





**Figure 6.** Satellite time series for Cordón Caulle volcano, Chile. See Figure 2 caption for details about symbols. Each of these data sets were collected from the points: CSK:  $-40.492, -72.211$ ; sentinel:  $-40.495, -72.185$ . ALOS data based on Jay et al. (2014) and Envisat 2003–2006 data based on Fournier et al. (2010). Envisat data from 6/1/11 to 3/13/12 generated through the use of a Yang model (Yang et al., 1988) to calculate the deformation at the crater due to decorrelation surrounding the main vent in during eruption caused by flows. All data sets with open points are interpolated from the general displacement trend of the data and do not represent the measured displacements values of the data points. The light blue area of the deformation graph marks the time over which the rate of any magmatic deformation is thought to be below the measurement threshold; any measured variability is believed to be the result of atmospheric interference. After the ASTER acquisition on 5/17/2011, the hottest thermal anomaly shifts from Los Baños geothermal area to the newly generated vent of the 6/4/2011 eruption. The vertical red line signifies the timing of the 4 June 2011 VEI 3 eruption.

27 days before eruption by Jay et al. (2014) (although see Euillades et al., 2017). In each of these cases, multiple data points were available shortly before the eruption, providing enough data to establish a change in the trend of the observed pre-eruptive parameters. *This reinforces the importance of having regular data acquisitions with a short temporal interval.* Additionally, these finding suggest that pre-eruptive unrest is unlikely to manifest in every data type, as only one eruption among the 20 inspected produced an identifiable pre-eruptive change in trend in all three. This reiterates the need for observations from multiple data types, including ground-based monitoring and established communication lines between volcano observatories and the satellite remote sensing community, and implies that imaging a volcano over multiple eruption and unrest cycles is necessary to fully understand how unrest can lead to eruption (or not).

### 4.3. Regional Trends

By plotting the system classifications and data values of these volcanoes on an area map of Latin America (Figure 7), some regional trends in volcano classification emerge. For example, Central America and Peru



**Figure 7.** Location and system classification of all 47 volcanoes in this study based on the information in Figure 3.

have mostly open volcanic systems, while the Galapagos Islands have only closed systems. In the Central Andes, there are open systems north of  $-22^{\circ}\text{S}$ , but closed systems dominate south of this latitude. These differences between the Central Andes and Central America were noted by Ebmeier et al. (2013a, 2013ab). They determined whether ground deformation in different volcanic arcs was greater or less than what would be expected based on the global distribution of volcanoes with both eruptions and deformation. Their study found that the Central Andes had more deformation than expected; this is consistent with the dominantly closed classification in this region found in our study. Further, Central America had less deformation than expected, consistent with the dominantly open classification in our study. Various explanations have been offered for these types of regional trends. For instance, Biggs et al. (2014) emphasize the role of regional variations in magma composition (basalt and andesite vs. rhyolite/dacite) and volcano type (calderas, stratocones, and shields) while Chaussard and Amelung (2014) propose that the upper crustal structure and tectonic stress are dominant controls. Future work will test these proposals for the driving forces of regional variations in classification when global data spanning a longer time period is available.

## 5. Recommendations and Conclusions

By integrating the satellite data acquired through multiple techniques over 17 years, we generated a more comprehensive representation of the behavior of 47 of the most active Latin American volcanoes than was previously possible with satellite data. Although a lack of data availability affects the ability to interpret the measured activity, a new understanding of the behavior of each volcano included in this study can be derived from a majority of these plots. By analyzing different types of data together, we can see not just how a certain type of behavior would influence a singular data type, but how the volcanic system is influenced as a whole. For example, once the crater lake begins to episodically evaporate at Copahue, passive SO<sub>2</sub> degassing increased, and thermal output became more variable (Figure 2). These data can also provide background information for each volcano included in this study. If, in the future, a potentially concerning detection is made at any of these volcanoes, 17 years of remote sensing material is now available as reference material, and the raw data are publically available through WOVODat (<http://www.wovodat.org/>).

These data are not only useful when analyzing individual volcanoes, but data collected for the entire region provides information on the relation between different types of unrest and eruption at different volcanoes. For example, the inadequacies in the established concepts of open and closed systems only become clear when observed in the time series for several volcanoes. These data then enabled us to measure how volcanic characteristics vary across the spectrum of open and closed volcanic systems. After analyzing all 47 volcanoes, 13 volcanoes could not be classified as either open or closed. Additionally, of the remaining volcanoes, many had varying degrees of open or closed behaviors. This suggests that rather than being a classification that all volcanoes must fall into, the open and closed ideals are more end-members in a spectrum of dynamic systems.

This is the first time multiple types of satellite observations have been directly compared on a regional basis for volcanoes. Where thermal data are available with both ASTER and MIROVA data types, they track the same general trends in thermal output. Additionally, the two data sets are complementary to each other, the increased temporal resolution of MIROVA provides a more accurate measurement of thermal trends with high thermal output, and the increased sensitivity of ASTER provides low thermal resolution measurements missed by MIROVA.

Integrating data for each of the 47 volcanoes in this study demonstrates how analyzing several different satellite-sensor techniques in parallel improves understanding of the behavior occurring at these volcanoes and stresses the need for a multitechnique analysis at other volcanoes. Sections 3.2 and 4.2 have demonstrated that it is common for precursory behavior to be expressed in one form of unrest but not another, dependent upon the type of volcanic system. Therefore, in order to monitor the full spectrum of volcanic activity each of these techniques should be included and would ideally be coupled with ground-based data (e.g., seismic monitoring, in situ observations).

This study also revealed that these remote sensing techniques are not being fully exploited. Despite collecting all available satellite-based degassing, thermal, and deformation data over 17 years, several volcanoes had time series plots that were incomplete and thus could not be easily interpreted. In some cases, (e.g., Galeras, Figure 6) we simply lack the temporal resolution needed to determine if a measurable change was related to eruption. This emphasized to us the need to collect these data with the highest possible temporal resolution. Only with enough consistently acquired data can satellite based instruments identify and classify the typical behavior of a volcanic system, such as whether regional variations in composition or tectonic stress play a role in different pre-eruptive trends. Environmental factors will always limit the quantity of clear and interpretable acquisitions. Nevertheless, the operational limits currently in place on the acquisition of thermal and deformation data do not allow the maximum efficiency of these sensors to be achieved. This is important to consider in the near future, as automated processing systems for deformation data such as COMET, SARVIEWS, and Aria (Hua et al., 2013; Meyer et al., 2016; Spaans et al., 2017) are now being implemented. Shortly, relevant phenomena will be observed with next-generation instruments that will improve the accuracy and/or utility of all the measurements used in this study in development: TROPOMI for degassing (Veeffkind et al., 2012), HypSIRI/SBG for thermal and degassing (Lee et al., 2015), and NISAR for deformation (Alvarez-Salazar et al., 2014). The advent of these sensors and systems is expected to provide an improvement in the quality and quantity of remotely sensed data available to volcanologists. However, to properly utilize these data, international coordination within the volcano remote sensing community will be necessary, including the routine creation of multisensor time series plots like those used in this study.

## Acknowledgments

This work was conducted as a part of the Volcano Remote Sensing Working Group supported by the John Wesley Powell Center for Analysis and Synthesis, funded in part by the U.S. Geological Survey. K. R., A. A., S. M., and M. E. P. were partly supported by NNX16AK87G issued through NASA's Science Mission Directorates Earth Science Division. A. A. and S. M. were also supported by a grant from the Cornell University Engineering Learning Initiatives. S. K. E. acknowledges support from the European Space Agency Fellowship, the Leverhulme Trust Early Career Fellowship, and from STREVA (NERC Grant NE/J020052/1), especially for supporting visits to the Instituto Geofísico, Ecuador. J. B. and S. K. E. were supported by NERC's Centre for the Observations and Modelling of Earthquakes, Volcanoes and Tectonics (COMET). C. W. was supported by NNX17AD70G issued through NASA's Science Mission Directorates Earth Science Division and NSF RAPID EAR 1620977. F. D. acknowledges CONICYT-Becas Chile for a PhD scholarship, NASA for the Earth and Space Sciences Graduate Research Fellowship, and the JPL Strategic University Research Partnership program. We acknowledge the CEOS volcano pilot project and the space agencies that provided data: Agenzia Spaziale Italiana (ASI) for CSK data, the German Space Agency for TSX/TDX data, the Canadian Space Agency (CSA), MacDonald, Dettwiler and Associates (MDA) Ltd. and the SOAR program for RSAT2 data, the European Space Agency for Sentinel data, NASA and LPDAAC for the ASTER and MODIS data, and the Japanese Aerospace Space Agency for ALOS-2 data. MIROVA is a collaborative project between the Universities of Turin and Florence (Italy) based on MODIS data provided by the LANCE-MODIS system. TanDEM-X DEM provided through proposal DEM\_GEOL2437 to F. D. We acknowledge Cunren Liang and Eric Fielding for help with the ALOS-2 processor. We thank Rowena Lohman and Alex Styler for discussions. We thank the many authors who contributed time series from their published papers: Anieri Morales, Nicole Richter, Helene Le Mevel, Eugenio Sansosti, Joel Ruch, Lauren Schaefer, Jackie Salzer, and Kirsten Stephens. Thank you to reviewers John Pallister and David Pieri as well as associate editor Martha Savage for improving the quality of this paper. The raw data used in producing these time series are publically available through WOVodat (<http://www.wovodat.org/>) data table can be found at <https://doi.org/10.25921/e9h5-ke08> (the following citations are included in the supplementary information: Aiuppa et al., 2010; Anderson & Segall, 2011;

## References

- Abrams, M., Hook, S., & Ramachandran, B. (2002). ASTER user handbook version 2. Jet Propulsion Laboratory. Retrieved from [http://ftp.gplf.umd.edu/library/pdf/aster\\_user\\_guide\\_v2.pdf](http://ftp.gplf.umd.edu/library/pdf/aster_user_guide_v2.pdf)
- Agusto, M., Tassi, F., Caselli, A. T., Vaselli, O., Rouwet, D., Capaccioni, B., et al. (2013). Gas geochemistry of the magmatic-hydrothermal fluid reservoir in the Copahue–Caviahue Volcanic Complex (Argentina). *Journal of Volcanology and Geothermal Research*, 257, 44–56. <https://doi.org/10.1016/j.jvolgeores.2013.03.003>
- Aiuppa, A., Bertagnini, A., Métrich, N., Moretti, R., Di Muro, A., Liuzzo, M., & Tamburello, G. (2010). A model of degassing for Stromboli volcano. *Earth and Planetary Science Letters*, 295(1–2), 195–204. <https://doi.org/10.1016/j.epsl.2010.03.040>
- Alvarez-Salazar, O., Hatch, S., Rocca, J., Rosen, P., Shaffer, S., Shen, Y., et al. (2014). *Sensors, Systems, and Next-Generation Satellites XVIII* (Vol. 9241, p. 92410C). International Society for Optics and Photonics. <https://doi.org/10.1117/12.2074162>
- Anderson, K., & Segall, P. (2011). Physics-based models of ground deformation and extrusion rate at effusively erupting volcanoes. *Journal of Geophysical Research*, 116, B07204. <https://doi.org/10.1029/2010JB007939>
- Arnold, D. W. D., Biggs, J., Anderson, K., Vallejo Vargas, S., Wadge, G., Ebmeier, S. K., et al. (2017). Decaying lava extrusion rate at El Reventador Volcano, Ecuador, measured using high-resolution satellite radar. *Journal of Geophysical Research: Solid Earth*, 122, 9966–9988. <https://doi.org/10.1002/2017JB014580>
- Arnold, D. W. D., Biggs, J., Wadge, G., Ebmeier, S. K., Odbert, H. M., & Poland, M. P. (2016). Dome growth, collapse, and valley fill at Soufrière Hills Volcano, Montserrat, from 1995 to 2013: Contributions from satellite radar measurements of topographic change. *Geosphere*, 12(4), 1300–1315. <https://doi.org/10.1130/GES01291.1>
- Bagnardi, M. (2014). Dynamics of magma supply, storage and migration at basaltic volcanoes: Geophysical studies of the Galápagos and Hawaiian Volcanoes. Open Access Dissertations. Retrieved from [http://scholarlyrepository.miami.edu/oa\\_dissertations/1179](http://scholarlyrepository.miami.edu/oa_dissertations/1179)
- Bagnardi, M., & Amelung, F. (2012). Space-geodetic evidence for multiple magma reservoirs and subvolcanic lateral intrusions at Fernandina Volcano, Galápagos Islands. *Journal of Geophysical Research*, 117, B10406. <https://doi.org/10.1029/2012JB009465>
- Baker, S. (2012). Investigating the dynamics of basaltic volcano magmatic systems with space geodesy. Open Access Dissertations. Retrieved from [https://scholarlyrepository.miami.edu/oa\\_dissertations/917](https://scholarlyrepository.miami.edu/oa_dissertations/917)
- Bally, P. (2012). Scientific and technical memorandum of the international forum on satellite EO and geohazards. European Space Agency Publication, 21–23, 170.
- Barberi, F., Corrado, G., Innocenti, F., & Luongo, G. (1984). Phlegraean fields 1982–1984: Brief chronicle of a volcano emergency in a densely populated area. *Bulletin Volcanologique*, 47, 175–185. Retrieved from <http://link.springer.com/article/10.1007/BF01961547>
- Barnhart, W. D., & Lohman, R. B. (2013). Characterizing and estimating noise in InSAR and InSAR time series with MODIS. *Geochemistry, Geophysics, Geosystems*, 14, 4121–4132. <https://doi.org/10.1002/ggge.20258>
- Berardino, P., Fornaro, G., Lanari, R., & Sansosti, E. (2002). A new algorithm for surface deformation monitoring based on small baseline differential SAR interferograms. *IEEE Transactions on Geoscience and Remote Sensing*, 40(11), 2375–2383. <https://doi.org/10.1109/TGRS.2002.803792>
- Biggs, J., Ebmeier, S. K., Aspinall, W. P., Lu, Z., Pritchard, M. E., Sparks, R. S. J., & Mather, T. A. (2014). Global link between deformation and volcanic eruption quantified by satellite imagery. *Nature Communications*, 5(1), 3471. <https://doi.org/10.1038/ncomms4471>
- Biggs, J., & Pritchard, M. (2017). Global volcano monitoring: What does it mean when volcanoes deform? *Elements*, 22. <https://doi.org/10.2113/gselements.13.1.17> Retrieved from <http://elements.gesocietymuseum.org/content/13/1/17.abstract>
- Blong, R. J. (2013). *Volcanic hazards: A sourcebook on the effects of eruptions*. Orlando, FL: Elsevier. Retrieved from [https://books.google.com/books?hl=en&lr=&id=6kjgBAAAQBAJ&oi=fnd&pg=PP1&dq=vocanic+hazards&ots=eBaF6sz\\_YW&sig=35nktgJTKJmcQ38xev3oF\\_LME4#v=onepage&q=vocanic+hazards&f=false](https://books.google.com/books?hl=en&lr=&id=6kjgBAAAQBAJ&oi=fnd&pg=PP1&dq=vocanic+hazards&ots=eBaF6sz_YW&sig=35nktgJTKJmcQ38xev3oF_LME4#v=onepage&q=vocanic+hazards&f=false)
- Bonali, F. L. (2013). Earthquake-induced static stress change on magma pathway in promoting the 2012 Copahue eruption. *Tectonophysics*, 608, 127–137. <https://doi.org/10.1016/j.tecto.2013.10.006>
- Bonny, E., & Wright, R. (2017). Predicting the end of lava flow-forming eruptions from space. *Bulletin of Volcanology*, 79(7), 52. <https://doi.org/10.1007/s00445-017-1134-8>
- Brown, S. K., Auker, M. R., & Sparks, R. S. J. (2015). Chapter 4 populations around holocene volcanoes and development of a population exposure index. *Global Volcanic Hazards and Risk* (pp. 223–232). Cambridge University Press. <https://doi.org/10.1017/CBO9781316276273.006>
- Brown, S. K., Sparks, R. S. J., Mee, K., Vye-Brown, C., Ilyinskaya, E., Jenkins, S. F., & Loughlin, S. C. (2015). Country and regional profiles of volcanic hazard and risk. *Global Volcanic Hazards and Risk*. <https://doi.org/10.1017/CBO9781316276273>
- Bruce, P. M., & Huppert, H. E. (1989). Thermal control of basaltic fissure eruptions. *Nature*, 342(6250), 665–667. <https://doi.org/10.1038/342665a0>
- Caltabiano, T., Romano, R., & Budetta, G. (1994). SO<sub>2</sub> flux measurements at Mount Etna (Sicily). *Journal of Geophysical Research*, 99(D6), 12809. <https://doi.org/10.1029/94JD00224>
- Cameron, C. E., Prejean, S. G., Coombs, M. L., Wallace, K. L., Power, J. A., & Roman, D. C. (2018). Alaska volcano observatory alert and forecasting timeliness: 1989–2017. *Frontiers in Earth Science*, 6, 86. <https://doi.org/10.3389/feart.2018.00086>
- Carn, S., Clarisse, L., & Prata, A. (2016). Multi-decadal satellite measurements of global volcanic degassing. *Journal of Volcanology and Geothermal Research*, 311, 99–134. <https://doi.org/10.1016/j.jvolgeores.2016.01.002>. Retrieved from <http://www.sciencedirect.com/science/article/pii/S0377027316000032>
- Carn, S., Krueger, A., & Bluth, G. (2003). Volcanic eruption detection by the total ozone mapping spectrometer (TOMS) instruments: A 22-year record of sulphur dioxide and ash emissions. *Geological Society*, 202. <https://doi.org/10.1144/GSL.SP.2003.213.01.11>. Retrieved from <http://sp.lyellcollection.org/content/213/1/11/short>
- Carn, S. A., Fioletov, V. E., McLinden, C. A., Li, C., & Krotkov, N. A. (2017). A decade of global volcanic SO<sub>2</sub> emissions measured from space. *Scientific Reports*, 7(1), 44095. <https://doi.org/10.1038/srep44095>
- Carn, S. A., Krotkov, N. A., Yang, K., & Krueger, A. J. (2013). Measuring global volcanic degassing with the ozone monitoring instrument (OMI). *Geological Society, London, Special Publications*, 380(1), 229–257. <https://doi.org/10.1144/SP380.12>
- Carn, S. A., Krueger, A. J., Arellano, S., Krotkov, N. A., & Yang, K. (2008). Daily monitoring of Ecuadorian volcanic degassing from space. *Journal of Volcanology and Geothermal Research*, 176(1), 141–150. <https://doi.org/10.1016/j.jvolgeores.2008.01.029>
- Caselli, A., Agosto, M., Velez, M. L., Forte, P., Bengoa, C., Daga, R., et al. (2016). The 2012 Eruption, in Copahue Volcano. In *Volcanoes of the world* (pp. 61–77). Berlin, Heidelberg: Springer. [https://doi.org/10.1007/978-3-662-48005-2\\_4](https://doi.org/10.1007/978-3-662-48005-2_4)
- Caselli, A. T., Agosto, M., & Fazio, A. (2005). Cambios térmicos y geoquímicos del lago craterico del volcán Copahue (Neuquén): Posibles variaciones cíclicas del sistema volcánico. XVI Congreso Geológico Argentino, La Plata, Argentina, 1.
- Caselli, A. T., Velez, M. L., Agosto, M., Liccioli, C., & Vaselli, O. (2016). Prehistoric to Historic Volcanic Activity at Copahue Volcano. In *Volcanoes of the world* (pp. 49–59). Berlin, Heidelberg: Springer. [https://doi.org/10.1007/978-3-662-48005-2\\_3](https://doi.org/10.1007/978-3-662-48005-2_3)

- Arnold et al., 2016, 2017; Bagnardi, 2014; Bagnardi & Amelung, 2012; Baker, 2012; Barnhart & Lohman, 2013; Champenois et al., 2014; Chaussard et al., 2013; Delgado, 2018; Delgado et al., 2017; Delgado et al., 2014; Ebmeier et al., 2018; Ebmeier et al., 2013a, 2010; Ebmeier et al. (2013b); Ebmeier et al., 2012; Ebmeier et al., 2016; Feigl et al., 2014; Fournier et al., 2010; Henderson & Pritchard, 2013; Henderson et al., 2017; Holtkamp et al., 2011; Huppert & Woods, 2002; Jay, 2014; Jay et al., 2014; Jay et al., 2015; Lyons et al., 2014; Lau et al., 2018; Le Mével et al., 2016; Lundgren et al., 2017, 2015; Lyons et al., 2012; McCormick et al., 2013; McTigue, 1987; Mirzaee & Amelung, 2017; Morales et al., 2017; Morales et al., 2016; C.G. Newhall, 2007; Odbert et al., 2014; Pinel et al., 2011; Pritchard et al., 2014; Pritchard et al., 2013; Richter et al., 2018; Ruch et al., 2009; Salzer et al., 2014; L. Schaefer et al., 2016; Schaefer et al., 2017; Schaefer et al., 2015; Stephens & Wauthier, 2018; Velez et al., 2016; Wnuk & Wauthier, 2017; R. Wright, 2016; T. J. Wright, Parsons, et al., 2004; Yang et al., 1988).
- Champenois, J., Pinel, V., Baize, S., Audin, L., Jomard, H., Hooper, A., et al. (2014). Large-scale inflation of Tungurahua volcano (Ecuador) revealed by persistent scatterers SAR interferometry. *Geophysical Research Letters*, *41*, 5821–5828. <https://doi.org/10.1002/2014GL060956>
- Chaussard, E. (2016). Subsidence in the Parícutin lava field: Causes and implications for interpretation of deformation fields at volcanoes. *Journal of Volcanology and Geothermal Research*, *320*, 1–11. <https://doi.org/10.1016/j.jvolgeores.2016.04.009>
- Chaussard, E., & Amelung, F. (2014). Regional controls on magma ascent and storage in volcanic arcs. *Geochemistry, geophysics, geosystems*. Retrieved from <http://onlinelibrary.wiley.com/doi/10.1002/2013GC005216/full>, 15, 1407, 1418
- Chaussard, E., Amelung, F., & Aoki, Y. (2013). Characterization of open and closed volcanic systems in Indonesia and Mexico using InSAR time series. *Journal of Geophysical Research: Solid Earth*, *118*, 3957–3969. <https://doi.org/10.1002/jgrb.50288>
- Coppola, D., Laiolo, M., Cigolini, C., Donne, D. D., & Ripepe, M. (2016). Enhanced volcanic hot-spot detection using MODIS IR data: Results from the MIROVA system. *Geological Society, London, Special Publications*, *426*(1), 181–205. <https://doi.org/10.1144/SP426.5>
- Coppola, D., Piscopo, D., Staudacher, T., & Cigolini, C. (2009). Lava discharge rate and effusive pattern at Piton de la Fournaise from MODIS data. *Journal of Volcanology and Geothermal Research*, *184*(1–2), 174–192. <https://doi.org/10.1016/j.jvolgeores.2008.11.031>
- Coppola, D., Ripepe, M., Laiolo, M., & Cigolini, C. (2017). Modelling satellite-derived magma discharge to explain caldera collapse. *Geology*, *45*(6), 523–526. <https://doi.org/10.1130/G38866.1>
- Dehn, J., Dean, K. G., Engle, K., & Izbekov, P. (2002). Thermal precursors in satellite images of the 1999 eruption of Shishaldin Volcano. *Bulletin of Volcanology*, *64*(8), 525–534. <https://doi.org/10.1007/s00445-002-0227-0>
- Delgado, F. (2018). Magma storage, transport, and eruption dynamics in the Southern Andean volcanic zone imaged with InSAR geodesy. Cornell University Dissertation.
- Delgado, F., Pritchard, M., Lohman, R., & Naranjo, J. A. (2014). The 2011 Hudson volcano eruption (Southern Andes, Chile): Pre-eruptive inflation and hotspots observed with InSAR and thermal imagery. *Bulletin of Volcanology*, *76*(5), 1–19. <https://doi.org/10.1007/s00445-014-0815-9>
- Delgado, F., Pritchard, M. E., Ebmeier, S., González, P., & Lara, L. (2017). Recent unrest (2002–2015) imaged by space geodesy at the highest risk Chilean volcanoes: Villarrica, Llaima, and Calbuco (Southern Andes). *Journal of Volcanology and Geothermal Research*, *344*, 270–288. <https://doi.org/10.1016/j.jvolgeores.2017.05.020>
- Ebmeier, S. K., Andrews, B., Araya, M. C., Arnold, D. W. D., Biggs, J., Cooper, C., et al. (2018). Synthesis of global volcano deformation observations: implications for volcano monitoring & the lateral extent of magmatic systems. *Journal of Applied Volcanology*, *7*. <https://doi.org/10.1186/s13617-018-0071-3>
- Ebmeier, S. K., Biggs, J., Mather, T. a., & Amelung, F. (2013a). Applicability of InSAR to tropical volcanoes: Insights from Central America. *Geological Society, London, Special Publications*, *380*(1), 15–37. <https://doi.org/10.1144/SP380.2>
- Ebmeier, S. K., Biggs, J., Mather, T. A., & Amelung, F. (2013b). On the lack of InSAR observations of magmatic deformation at Central American volcanoes. *Journal of Geophysical Research: Solid Earth*, *118*, 2571–2585. <https://doi.org/10.1002/jgrb.50195>
- Ebmeier, S. K., Biggs, J., Mather, T. A., Elliott, J. R., Wadge, G., & Amelung, F. (2012). Measuring large topographic change with InSAR: Lava thicknesses, extrusion rate and subsidence rate at Santiaguito volcano, Guatemala. *Earth and Planetary Science Letters*, *335–336*, 216–225. <https://doi.org/10.1016/j.epsl.2012.04.027>
- Ebmeier, S. K., Biggs, J., Mather, T. A., Wadge, G., & Amelung, F. (2010). Steady downslope movement on the western flank of Arenal volcano, Costa Rica. *Geochemistry, Geophysics, Geosystems*, *11*, Q12004. <https://doi.org/10.1029/2010GC003263>
- Ebmeier, S. K., Elliott, J. R., Nocquet, J.-M., Biggs, J., Mothes, P., Jarrin, P., et al. (2016). Shallow earthquake inhibits unrest near Chiles–Cerro Negro volcanoes, Ecuador–Colombian border. *Earth and Planetary Science Letters*, *450*, 283–291. <https://doi.org/10.1016/j.epsl.2016.06.046>
- Euillades, P. A., Euillades, L. D., Blanco, M. H., Velez, M. L., Grosse, P., & Sosa, G. J. (2017). Co-eruptive subsidence and post-eruptive uplift associated with the 2011–2012 eruption of Puyehue-Cordón Caulle, Chile, revealed by DInSAR. *Journal of Volcanology and Geothermal Research*, *344*, 257–269. <https://doi.org/10.1016/j.jvolgeores.2017.06.023>
- Feigl, K. L., Le Mével, H., Tabrez Ali, S., Córdova, L., Andersen, N. L., DeMets, C., & Singer, B. S. (2014). Rapid uplift in Laguna del Maule volcanic field of the Andean Southern Volcanic zone (Chile) 2007–2012. *Geophysical Journal International*, *196*(2), 885–901. <https://doi.org/10.1093/gji/ggt438>
- Fournier, T. J., Pritchard, M. E., & Riddick, S. N. (2010). Duration, magnitude, and frequency of subaerial volcano deformation events: New results from Latin America using InSAR and a global synthesis. *Geochemistry, Geophysics, Geosystems*, *11*, Q01003. <https://doi.org/10.1029/2009GC002558>
- Francis, P. W., & Rothery, D. A. (1987). Using the Landsat Thematic Mapper to detect and monitor active volcanoes: An example from Lascar volcano, northern Chile. *Geology*, *15*(7), 614. [https://doi.org/10.1130/0091-7613\(1987\)15<614:UJLTMT>2.0.CO;2](https://doi.org/10.1130/0091-7613(1987)15<614:UJLTMT>2.0.CO;2)
- Galle, B., Johansson, M., Rivera, C., Zhang, Y., Kihlman, M., Kern, C., et al. (2010). Network for observation of volcanic and atmospheric change (NOVAC)—A global network for volcanic gas monitoring: Network layout and instrument description. *Journal of Geophysical Research*, *115*, D05304. <https://doi.org/10.1029/2009JD011823>
- Geist, D. J., Naumann, T. R., Standish, J. J., Kurz, M. D., Harpp, K. S., White, W. M., & Fornari, D. J. (2005). Wolf Volcano, Galápagos Archipelago: Melting and magmatic evolution at the margins of a mantle plume. *Journal of Petrology*, *46*(11), 2197–2224. <https://doi.org/10.1093/ptrology/egj052>
- Gillespie, A., Rokugawa, S., & Matsunaga, T. (1998). A temperature and emissivity separation algorithm for advanced spaceborne thermal emission and reflection radiometer (ASTER) images. *Transactions on IEEE*, *36*(4), 1113–1126. <https://doi.org/10.1109/36.700995>. Retrieved from <http://ieeexplore.ieee.org/abstract/document/700995/>
- Girona, T., Costa, F., & Schubert, G. (2015). Degassing during quiescence as a trigger of magma ascent and volcanic eruptions. *Scientific Reports*, *5*. <https://doi.org/10.1038/srep18212>
- Harris, A. J. L., Flynn, L. P., Keszthelyi, L., Mouginiis-Mark, P. J., Rowland, S. K., & Resing, J. A. (1998). Calculation of lava effusion rates from Landsat TM data. *Bulletin of Volcanology*, *60*(1), 52–71. <https://doi.org/10.1007/s004450050216>
- Harris, A. J. L., Murray, J. B., Aries, S. E., Davies, M. A., Flynn, L. P., Wooster, M. J., et al. (2000). Effusion rate trends at Etna and Krafla and their implications for eruptive mechanisms. *Journal of Volcanology and Geothermal Research*, *102*(3–4), 237–269. [https://doi.org/10.1016/S0377-0273\(00\)00190-6](https://doi.org/10.1016/S0377-0273(00)00190-6)
- Henderson, S. T., Delgado, F., Elliott, J., Pritchard, M. E., & Lundgren, P. R. (2017). Decelerating uplift at Lazufre volcanic center, Central Andes, from A.D. 2010 to 2016, and implications for geodetic models. *Geosphere*, *13*(5), 1489–1505. <https://doi.org/10.1130/GES01441.1>
- Henderson, S. T., & Pritchard, M. E. (2013). Decadal volcanic deformation in the Central Andes Volcanic Zone revealed by InSAR time series. *Geochemistry, Geophysics, Geosystems*, *14*, 1358–1374. <https://doi.org/10.1002/ggge.20074>

- Holtkamp, S. G., Pritchard, M. E., & Lohman, R. B. (2011). Earthquake swarms in South America. *Geophysical Journal International*, 187(1), 128–146. <https://doi.org/10.1111/j.1365-246X.2011.05137.x>
- Hua, H., Owen, S. E., Yun, S., Lundgren, P., Fielding, E. J., Agram, P., et al. (2013). Integrating remote sensing data, hybrid-cloud computing, and event notifications for advanced rapid imaging & analysis (invited). *American Geophysical Union, Fall Meeting 2013, Abstract Id. IN23E-06*. Retrieved from <http://adsabs.harvard.edu/abs/2013AGUFMIN23E..06H>
- Huppert, H. E., & Woods, A. W. (2002). The role of volatiles in magma chamber dynamics. *Nature*, 420(6915), 493–495. <https://doi.org/10.1038/nature01211>
- Ibáñez, J. M., Del Pezzo, E., Bengoa, C., Caselli, A., Badi, G., & Almendros, J. (2008). Volcanic tremor and local earthquakes at Copahue volcanic complex, Southern Andes, Argentina. *Journal of Volcanology and Geothermal Research*, 174(4), 284–294. <https://doi.org/10.1016/j.jvolgeores.2008.02.005>
- Jay, J. (2014). A geophysical survey of active volcanism in the Central and Southern Andes. *Cornell University*, (May).
- Jay, J., Costa, F., Pritchard, M., Lara, L., Singer, B., & Herrin, J. (2014). Locating magma reservoirs using InSAR and petrology before and during the 2011–2012 Cordón Caulle silicic eruption. *Earth and Planetary Science Letters*, 395, 254–266. <https://doi.org/10.1016/j.epsl.2014.03.046>
- Jay, J. A., Delgado, F. J., Torres, J. L., Pritchard, M. E., Macedo, O., & Aguilar, V. (2015). Deformation and seismicity near Sabancaya volcano, southern Peru, from 2002 to 2015. *Geophysical Research Letters*, 42, 2780–2788. <https://doi.org/10.1002/2015GL063589>
- Jay, J. A., Welch, M., Pritchard, M. E., Mares, P. J., Mnich, M. E., Melkonian, A. K., et al. (2013). Volcanic hotspots of the central and southern Andes as seen from space by ASTER and MODVOLC between the years 2000 and 2010. *Geological Society Special Publication*, 380(1), 161–185. <https://doi.org/10.1144/SP380.1>
- Kaneko, T., & Wooster, M. J. (1999). Landsat infrared analysis of fumarole activity at Unzen volcano: Time-series comparison with gas and magma fluxes. *Journal of Volcanology and Geothermal Research*, 89(1–4), 57–64. [https://doi.org/10.1016/S0377-0273\(98\)00122-X](https://doi.org/10.1016/S0377-0273(98)00122-X)
- Kauhikaua, J., & Poland, M. (2012). One hundred years of volcano monitoring in Hawaii. *Eos, Transactions American Geophysical Union*, 93(3), 29–30. <https://doi.org/10.1029/2012EO030001>
- Kouamé, J. L., Frison, P. L., Mascaret, A., & Rudant, J. P. (2006). Evaluation of the potential of SAR ERS and ASAR ENVISAT sensors in multi-incidence and multi-polarisation modes for landscape study in French Guyana: Examples of Kourou and Saint Laurent du Maroni WGS I/1, 1/2, 1/6. *Revue Française de Photogrammétrie et de Télédétection*, 182, 53–59. Retrieved from <http://citeseerx.ist.psu.edu/viewdoc/download?doi=10.1.1.437.6786&rep=rep1&type=pdf>
- Lau, N., Tymofyeyeva, E., & Fialko, Y. (2018). Variations in the long-term uplift rate due to the Altiplano–Puna magma body observed with Sentinel-1 interferometry. *Earth and Planetary Science Letters*, 491, 43–47. <https://doi.org/10.1016/j.epsl.2018.03.026>
- Le Mével, H., Gregg, P. M., & Feigl, K. L. (2016). Magma injection into a long-lived reservoir to explain geodetically measured uplift: Application to the 2007–2014 unrest episode at Laguna del Maule volcanic field, Chile. *Journal of Geophysical Research: Solid Earth*, 121, 6092–6108. <https://doi.org/10.1002/2016JB013066>
- Lee, C. M., Cable, M. L., Hook, S. J., Green, R. O., Ustin, S. L., Mandl, D. J., & Middleton, E. M. (2015). An introduction to the NASA Hyperspectral InfraRed Imager (HyspIRI) mission and preparatory activities. *Remote Sensing of Environment*, 167, 6–19. <https://doi.org/10.1016/j.rse.2015.06.012>
- Loughlin, S. C., Vye-Brown, C., Sparks, R. S. J., Brown, S. K., Barclay, J., Calder, E., et al. (2015). *Chapter 1 an introduction to global volcanic hazard and risk*. Cambridge University Press. <https://doi.org/10.1017/CBO9781316276273.003>
- Lu, Z., Dzurisin, D., Biggs, J., Wicks, C., & McNutt, S. (2010). Ground surface deformation patterns, magma supply, and magma storage at Okmok volcano, Alaska, from InSAR analysis: 1. Interruption deformation, 1997–2008. *Journal of Geophysical Research*, 115, B00B02. <https://doi.org/10.1029/2009JB006969>
- Lucas, R., Armston, J., Fairfax, R., Fensham, R., Accad, A., Carreiras, J., et al. (2010). An evaluation of the ALOS PALSAR L-band backscatter—Above ground biomass relationship Queensland, Australia: Impacts of surface moisture condition and vegetation structure. *IEEE Journal of Selected Topics in Applied Earth Observations and Remote Sensing*, 3(4), 576–593. <https://doi.org/10.1109/JSTARS.2010.2086436>
- Lundgren, P., Nikkhoo, M., Samsonov, S. V., Milillo, P., Gil-Cruz, F., & Lazo, J. (2017). Source model for the Copahue volcano magma plumbing system constrained by InSAR surface deformation observations. *Journal of Geophysical Research: Solid Earth*, 122, 5729–5747. <https://doi.org/10.1002/2017JB014368>
- Lundgren, P., Samsonov, S. V., López Velez, C. M., & Ordoñez, M. (2015). Deep source model for Nevado del Ruiz Volcano, Colombia, constrained by interferometric synthetic aperture radar observations. *Geophysical Research Letters*, 42, 4816–4823. <https://doi.org/10.1002/2015GL063858>
- Lyons, J. J., Waite, G. P., Ichihara, M., & Lees, J. M. (2012). Tilt prior to explosions and the effect of topography on ultra-long-period seismic records at Fuego volcano, Guatemala. *Geophysical Research Letters*, 39, L08305. <https://doi.org/10.1029/2012GL051184>
- McCormick, B. T., Edmonds, M., Mather, T. A., Campion, R., Hayer, C. S. L., Thomas, H. E., & Carn, S. A. (2013). Volcano monitoring applications of the ozone monitoring instrument. *Geological Society, London, Special Publications*, 380(1), 259–291. <https://doi.org/10.1144/SP380.11>
- McTigue, D. F. (1987). Elastic stress and deformation near a finite spherical magma body: Resolution of the point source paradox. *Journal of Geophysical Research*, 92(B12), 12931. <https://doi.org/10.1029/JB092iB12p12931>
- Meyer, F. J., Webley, P. W., Dehn, J., Arko, S. A., McAlpin, D. B., & Gong, W. (2016). The SARVIEWS project: Automated SAR processing in support of operational near real-time volcano monitoring. *American Geophysical Union, Fall General Assembly 2016, Abstract Id. NH43D-02*. Retrieved from <http://adsabs.harvard.edu/abs/2016AGUFMNH43D..02M>
- Mirzaee, S., & Amelung, F. (2017). What InSAR time-series methods are best suited for the Ecuadorian volcanoes. *American Geophysical Union, Fall Meeting 2017, Abstract #G23A-0891*. Retrieved from <http://adsabs.harvard.edu/abs/2017AGUFM.G23A0891M>
- Morales Rivera, A. M., Amelung, F., & Mothes, P. (2016). Volcano deformation survey over the Northern and Central Andes with ALOS InSAR time series. *Geochemistry, Geophysics, Geosystems*, 17, 2869–2883. <https://doi.org/10.1002/2016GC006393>
- Morales Rivera, A. M., Amelung, F., Mothes, P., Hong, S.-H., Nocquet, J.-M., & Jarrin, P. (2017). Ground deformation before the 2015 eruptions of Cotopaxi volcano detected by InSAR. *Geophysical Research Letters*, 44, 6607–6615. <https://doi.org/10.1002/2017GL073720>
- Moran, S. C., Kwoun, O., Masterlark, T., & Lu, Z. (2006). On the absence of InSAR-detected volcano deformation spanning the 1995–1996 and 1999 eruptions of Shishaldin Volcano, Alaska. *Journal of Volcanology and Geothermal Research*, 150(1–3), 119–131. <https://doi.org/10.1016/j.jvolgeores.2005.07.013>
- Mothes, P. A., Yepes, H. A., Hall, M. L., Ramón, P. A., Steele, A. L., & Ruiz, M. C. (2015). The scientific–community interface over the fifteen-year eruptive episode of Tungurahua Volcano, Ecuador. *Journal of Applied Volcanology*, 4(1), 9. <https://doi.org/10.1186/s13617-015-0025-y>

- Moussallam, Y., Bani, P., Curtis, A., Barnie, T., Moussallam, M., Peters, N., et al. (2016). Sustaining persistent lava lakes: Observations from high-resolution gas measurements at Villarrica volcano, Chile. *Earth and Planetary Science Letters*, *454*, 237–247. <https://doi.org/10.1016/j.epsl.2016.09.012>
- Naranjo, J. A., & Polanco, E. (2004). The 2000 AD eruption of Copahue Volcano, Southern Andes. *Revista Geologica de Chile*, *31*(2), 279–292. <https://doi.org/10.4067/S0716-02082004000200007>
- National Academies of Sciences, E. and M (2017). *Volcanic eruptions and their repose, unrest, precursors, and timing*. Washington, DC: National Academies Press. <https://doi.org/10.17226/24650>
- Newhall, C. G. (2000). Volcano warnings. In *Encyclopedia of Volcanoes* (pp. 1–85). New York: Academic Press.
- Newhall, C. G. (2007). Volcanology 101 for seismologists. In *Treatise on geophysics* (pp. 351–388). Amsterdam, Netherlands: Elsevier. <https://doi.org/10.1016/B978-044452748-6.00072-9>
- Newhall, C. G., Costa, F., Ratdomopurbo, A., Venezky, D. Y., Widiwijayanti, C., Win, N. T. Z., et al. (2017). WOVodat—An online, growing library of worldwide volcanic unrest. *Journal of Volcanology and Geothermal Research*, *345*, 184–199. <https://doi.org/10.1016/j.jvolgeores.2017.08.003>
- Newhall, C. G., & Self, S. (1982). The volcanic explosivity index (VEI) an estimate of explosive magnitude for historical volcanism. *Journal of Geophysical Research*, *87*(C2), 1231. <https://doi.org/10.1029/JC087iC02p01231>
- Odbert, H. M., Ryan, G. A., Mattioli, G. S., Hautmann, S., Gottsmann, J., Fournier, N., & Herd, R. A. (2014). Volcano geodesy at the Soufriere Hills Volcano, Montserrat: A review. *Geological Society, London, Memoirs*, *39*(1), 195–217. <https://doi.org/10.1144/M39.11>
- Oppenheimer, C., & Francis, P. (1997). Remote sensing of heat, lava and fumarole emissions from Erta'Ale volcano, Ethiopia. *International Journal of Remote Sensing*, *18*(8), 1661–1692. <https://doi.org/10.1080/014311697218043>
- Oppenheimer, C., Francis, P. W., Rothery, D. A., Carlton, R. W. T., & Glaze, L. S. (1993). Infrared image analysis of volcanic thermal features: Lascar volcano, Chile, 1984–1992. *Journal of Geophysical Research*, *98*(B3), 4269–4286. <https://doi.org/10.1029/92JB02134>
- Pallister, J. S., Schneider, D. J., Griswold, J. P., Keeler, R. H., Burton, W. C., Noyles, C., et al. (2012). Merapi 2010 eruption—Chronology and extrusion rates monitored with satellite radar and used in eruption forecasting. *Journal of Volcanology and Geothermal Research*, *261*, 144–152. <https://doi.org/10.1016/j.jvolgeores.2012.07.012>
- Parks, M. M., Biggs, J., Mather, T. A., Pyle, D. M., Amelung, F., Monsalve, M. L., & Medina, L. N. (2011). Co-eruptive subsidence at Galeras identified during an InSAR survey of Colombian volcanoes (2006–2009). *Journal of Volcanology and Geothermal Research*, *202*(3–4), 228–240. <https://doi.org/10.1016/j.jvolgeores.2011.02.007>
- Phillipson, G., Sobradelo, R., & Gottsmann, J. (2013). Global volcanic unrest in the 21st century: An analysis of the first decade. *Journal of Volcanology and Geothermal Research*, *264*, 183–196. <https://doi.org/10.1016/j.jvolgeores.2013.08.004>
- Pieri, D., & Abrams, M. (2005). ASTER observations of thermal anomalies preceding the April 2003 eruption of Chikurachki volcano, Kurile Islands, Russia. *Remote Sensing of Environment*, *99*(1–2), 84–94. <https://doi.org/10.1016/j.rse.2005.06.012>
- Pinel, V., Hooper, A., De la Cruz-Reyna, S., Reyes-Davila, G., Doin, M. P., & Bascou, P. (2011). The challenging retrieval of the displacement field from InSAR data for andesitic stratovolcanoes: Case study of Popocatepetl and Colima Volcano, Mexico. *Journal of Volcanology and Geothermal Research*, *200*(1–2), 49–61. <https://doi.org/10.1016/j.jvolgeores.2010.12.002>
- Pinel, V., Poland, M. P., & Hooper, A. (2014). Volcanology: Lessons learned from synthetic aperture radar imagery. *Journal of Volcanology and Geothermal Research*, *289*, 81–113. <https://doi.org/10.1016/j.jvolgeores.2014.10.010>
- Potter, S. H., Scott, B. J., Jolly, G. E., Neall, V. E., & Johnston, D. M. (2015). Introducing the volcanic unrest index (VUI): A tool to quantify and communicate the intensity of volcanic unrest. *Bulletin of Volcanology*, *77*(9). <https://doi.org/10.1007/s00445-015-0957-4>
- Pritchard, M., Henderson, S., Jay, J., Soler, V., Krzesni, D., Button, N., et al. (2014). Reconnaissance earthquake studies at nine volcanic areas of the Central Andes with coincident satellite thermal and InSAR observations. *Journal of Volcanology and Geothermal Research*, *280*, 90–103. <https://doi.org/10.1016/j.jvolgeores.2014.05.004>
- Pritchard, M. E., Biggs, J., Wauthier, C., Sansosti, E., Arnold, D. W. D., Delgado, F., et al. (2018). Towards coordinated regional multi-satellite InSAR volcano observations: Results from the Latin America pilot project. *Journal of Applied Volcanology*, *7*(1), 5. <https://doi.org/10.1186/s13617-018-0074-0>
- Pritchard, M. E., Jay, J. A., Aron, F., Henderson, S. T., & Lara, L. E. (2013). Subsidence at southern Andes volcanoes induced by the 2010 Maule, Chile earthquake. *Nature Geoscience*, *6*(8), 632–636. <https://doi.org/10.1038/ngeo1855>
- Pritchard, M. E., & Simons, M. (2004). An InSAR-based survey of volcanic deformation in the central Andes. *Geochemistry, Geophysics, Geosystems*, *5*, Q02002. <https://doi.org/10.1029/2003GC000610>
- Ramsey, M. S. (2016). Synergistic use of satellite thermal detection and science: A decadal perspective using ASTER. *Geological Society, London, Special Publications*, *426*(1), 115–136. <https://doi.org/10.1144/SP426.23>
- Reath, K. A., Ramsey, M. S., Dehn, J., & Webley, P. W. (2016). Predicting eruptions from precursory activity using remote sensing data hybridization. *Journal of Volcanology and Geothermal Research*, *321*, 18–30. <https://doi.org/10.1016/j.jvolgeores.2016.04.027>
- Richter, N., Salzer, J. T., de Zeeuw-van Dalfsen, E., Perissin, D., & Walter, T. R. (2018). Constraints on the geomorphological evolution of the nested summit craters of Lascar volcano from high spatio-temporal resolution TerraSAR-X interferometry. *Bulletin of Volcanology*, *80*(3), 21. <https://doi.org/10.1007/s00445-018-1195-3>
- Ridley, D. A., Solomon, S., Barnes, J. E., Burlakov, V. D., Deshler, T., Dolgii, S. I., et al. (2014). Total volcanic stratospheric aerosol optical depths and implications for global climate change. *Geophysical Research Letters*, *41*, 7763–7769. <https://doi.org/10.1002/2014GL061541>
- Ripepe, M., Pistolesi, M., Coppola, D., Delle Donne, D., Genco, R., Lacanna, G., et al. (2017). Forecasting effusive dynamics and decompression rates by magmatic model at open-vent volcanoes. *Scientific Reports*, *7*(1), 3885. <https://doi.org/10.1038/s41598-017-03833-3>
- Ruch, J., Manconi, A., Zeni, G., Solaro, G., Pepe, A., Shirzaei, M., et al. (2009). Stress transfer in the Lazufre volcanic area, Central Andes. *Geophysical Research Letters*, *36*, L22303. <https://doi.org/10.1029/2009GL041276>
- Salzer, J. T., Nikkhoo, M., Walter, T. R., Sudhaus, H., Reyes-Dávila, G., Bretón, M., & Arambula, R. (2014). Satellite radar data reveal short-term pre-explosive displacements and a complex conduit system at Volcan de Colima, Mexico. *Frontiers in Earth Science*, *2*. <https://doi.org/10.3389/feart.2014.00012>
- Schaefer, L., Lu, Z., & Oommen, T. (2016). Post-eruption deformation processes measured using ALOS-1 and UAVSAR InSAR at Pacaya Volcano, Guatemala. *Remote Sensing*, *8*(1), 73. <https://doi.org/10.3390/rs8010073>
- Schaefer, L. N., Lu, Z., & Oommen, T. (2015). Dramatic volcanic instability revealed by InSAR. *Geology*, *43*(8), 743–746. <https://doi.org/10.1130/G36678.1>
- Schaefer, L. N., Wang, T., Escobar-Wolf, R., Oommen, T., Lu, Z., Kim, J., et al. (2017). Three-dimensional displacements of a large volcano flank movement during the May 2010 eruptions at Pacaya Volcano, Guatemala. *Geophysical Research Letters*, *44*, 135–142. <https://doi.org/10.1002/2016GL071402>

- Segall, P. (2013). Volcano deformation and eruption forecasting. *Geological Society, London, Special Publications*, 106. <https://doi.org/10.1144/SP380.4>. Retrieved from <http://sp.lyellcollection.org/content/380/1/85.short>
- Shinohara, H., & Witter, J. B. (2005). Volcanic gases emitted during mild Strombolian activity of Villarrica volcano, Chile. *Geophysical Research Letters*, 32, L20308. <https://doi.org/10.1029/2005GL024131>
- Spaans, K., Hatton, E., Gonzalez, P., Walters, R., McDougall, A., Wright, T., & Hooper, A. (2017). Tectonic and volcanic monitoring using Sentinel-1: Current status and future plans of the COMET InSAR portal. *19th EGU General Assembly, EGU2017, Proceedings from the Conference Held 23-28 April, 2017 in Vienna, Austria, p.19397, 19, 19397*. Retrieved from <http://adsabs.harvard.edu/abs/2017EGUGA..1919397S>
- Sparks, R. (2003). Forecasting volcanic eruptions. *Earth and Planetary Science Letters*, 210(1-2), 1-15. [https://doi.org/10.1016/S0012-821X\(03\)00124-9](https://doi.org/10.1016/S0012-821X(03)00124-9). Retrieved from <http://www.sciencedirect.com/science/article/pii/S0012821X03001249>
- Stephens, K. J., & Wauthier, C. (2018). Satellite geodesy captures offset magma supply associated with lava lake appearance at Masaya volcano, Nicaragua. *Geophysical Research Letters*, 45, 2669-2678. <https://doi.org/10.1002/2017GL076769>
- Symonds, R., Rose, W., Bluth, G., & Gerlach, T. (1994). Volcanic-gas studies: Methods, results, and applications. In M. R. Carroll & J. R. Holloway (Eds.), *Volatiles in magma, Mineralogical Society of America Reviews in Mineralogy* (Vol. 30, pp. 1-66). Retrieved from <https://digitalcommons.mtu.edu/geo-fp/97>
- Theys, N., Campion, R., Clarisse, L., Brenot, H., van Gent, J., Dils, B., et al. (2013). Volcanic SO<sub>2</sub> fluxes derived from satellite data: A survey using OMI, GOME-2, IASI and MODIS. *Atmospheric Chemistry and Physics*, 13(12), 5945-5968. <https://doi.org/10.5194/acp-13-5945-2013>
- Varekamp, J. C., Ouimette, A. P., Herman, S. W., Bermúdez, A., & Delpino, D. (2001). Hydrothermal element fluxes from Copahue, Argentina: A "beehive" volcano in turmoil. *Geology*, 29(11), 1059. [https://doi.org/10.1130/0091-7613\(2001\)029<1059:HEFFCA>2.0.CO;2](https://doi.org/10.1130/0091-7613(2001)029<1059:HEFFCA>2.0.CO;2)
- Veeffkind, J. P., Aben, I., McMullan, K., Förster, H., De Vries, J., Otter, G., et al. (2012). TROPOMI on the ESA Sentinel-5 precursor: A GMES mission for global observations of the atmospheric composition for climate, air quality and ozone layer applications. *Remote Sensing of Environment*, 120, 70-83. <https://doi.org/10.1016/j.rse.2011.09.027>
- Velez, M. L., Euillades, P., Blanco, M., & Euillades, L. (2016). Ground deformation between 2002 and 2013 from InSAR observations. In F. Tassi, O. Vaselli, & A. Caselli (Eds.), *Copahue volcano* (pp. 175-198). Heidelberg: Springer. [https://doi.org/10.1007/978-3-662-48005-2\\_8](https://doi.org/10.1007/978-3-662-48005-2_8)
- Velez, M. L., Euillades, P., Caselli, A., Blanco, M., & Diaz, J. M. (2011). Deformation of Copahue volcano: Inversion of InSAR data using a genetic algorithm. *Journal of Volcanology and Geothermal Research*, 202(1-2), 117-126. <https://doi.org/10.1016/j.jvolgeores.2011.01.012>
- Venzke, E. (2013). Global volcanism program. Smithsonian Institution. Retrieved from <https://doi.org/10.5479/si.GVP.VOTW4-2013>
- Wadge, G., & Aspinall, W. P. (2014). Chapter 24 A review of volcanic hazard and risk-assessment praxis at the Soufriere Hills Volcano, Montserrat from 1997 to 2011. *Geological Society, London, Memoirs*, 39(1), 439-456. <https://doi.org/10.1144/M39.24>
- Wadge, G., Voight, B., Sparks, R. S. J., Cole, P. D., Loughlin, S. C., & Robertson, R. E. A. (2014). Chapter 1 An overview of the eruption of Soufriere Hills Volcano, Montserrat from 2000 to 2010. *Geological Society, London, Memoirs*, 39(1), 1.1-1.40. <https://doi.org/10.1144/M39.1>
- Wauthier, C., Roman, D. C., & Poland, M. P. (2013). Moderate-magnitude earthquakes induced by magma reservoir inflation at Kilauea Volcano, Hawai'i. *Geophysical Research Letters*, 40, 5366-5370. <https://doi.org/10.1002/2013GL058082>
- Wauthier, C., Smets, B., & Keir, D. (2015). Diking-induced moderate-magnitude earthquakes on a youthful rift border fault: The 2002 Nyiragongo-Kalehe sequence, D.R. Congo. *Geochemistry, Geophysics, Geosystems*, 16, 4280-4291. <https://doi.org/10.1002/2015GC006110>
- Wicks, C., de la Llera, J. C., Lara, L. E., & Lowenstern, J. (2011). The role of dyking and fault control in the rapid onset of eruption at Chaitén volcano, Chile. *Nature*, 478(7369), 374-377. <https://doi.org/10.1038/nature10541>
- Winson, A., Costa, F., Newhall, C., & Woo, G. (2014). An analysis of the issuance of volcanic alert levels during volcanic crises. *Journal of Applied*, 3(1). Retrieved from <http://link.springer.com/article/10.1186/s13617-014-0014-6>
- Wnuk, K., & Wauthier, C. (2017). Surface deformation induced by magmatic processes at Pacaya Volcano, Guatemala revealed by InSAR. *Journal of Volcanology and Geothermal Research*, 344, 197-211. <https://doi.org/10.1016/j.jvolgeores.2017.06.024>
- Wright, R. (2016). MODVOLC: 14 years of autonomous observations of effusive volcanism from space. *Geological Society, London, Special Publications*, 426(1), 23-53. <https://doi.org/10.1144/SP426.12>
- Wright, R., Flynn, L. P., Garbeil, H., Harris, A. J. L., & Pilger, E. (2004). MODVOLC: Near-real-time thermal monitoring of global volcanism. *Journal of Volcanology and Geothermal Research*, 135(1-2), 29-49. <https://doi.org/10.1016/j.jvolgeores.2003.12.008>
- Wright, T. J., Parsons, B. E., & Lu, Z. (2004). Toward mapping surface deformation in three dimensions using InSAR. *Geophysical Research Letters*, 31, L01607. <https://doi.org/10.1029/2003GL018827>
- Wunderman, R. (Ed.). (2008). Report on Chaitén (Chile). Bulletin of the Global Volcanism Network, 33(4). <https://doi.org/10.5479/si.GVP.BGVN200804-358041>
- Yamaguchi, Y., Kahle, A. B., Tsu, H., Kawakami, T., & Pniel, M. (1998). Overview of advanced spaceborne thermal emission and reflection radiometer (ASTER). *IEEE Transactions on Geoscience and Remote Sensing*, 36(4), 1062-1071. <https://doi.org/10.1109/36.700991>. Retrieved from [http://www.geo.mtu.edu/EHaz/VolcanoInstability\\_class/ramsey/pdf/Yamaguchi\\_etal\\_IEEE\\_36\\_1998\\_ASTERoverview.pdf](http://www.geo.mtu.edu/EHaz/VolcanoInstability_class/ramsey/pdf/Yamaguchi_etal_IEEE_36_1998_ASTERoverview.pdf)
- Yang, X.-M., Davis, P. M., & Dieterich, J. H. (1988). Deformation from inflation of a dipping finite prolate spheroid in an elastic half-space as a model for volcanic stressing. *Journal of Geophysical Research*, 93(B5), 4249-4257. <https://doi.org/10.1029/JB093iB05p04249>